SIMULATION OF ORIENTED PATTERNS WITH PRESCRIBED LOCAL ORIENTATION USING ANISOTROPIC GAUSSIAN FIELDS*

KÉVIN POLISANO†, MARIANNE CLAUSEL†, LAURENT CONDAT‡, AND VALÉRIE PERRIER†

Abstract. We consider a stochastic framework for oriented texture modeling. We study a large class of generalized Gaussian fields, called Generalized Anisotropic Fractional Brownian Fields (GAFBF), which combines a local version of an Anisotropic Fractional Brownian Fields (AFBF) with Multifractional Brownian Fields (MBF). This mixture enables to control both the local orientation and the roughness of the texture. A second model based on fields deformation and called Warped Anisotropic Fractional Brownian Fields (WAFBF) is also studied. In this paper, we first establish theoretical results of these new stochastic models, and describe their properties. The notion of orientation for localizable random fields we introduced in our previous works is relevant to give explicit formulas for the orientations of these two models, insuring the control of the expected one. Furthermore, we investigate different ways to simulate a collection of textures with prescribed local orientation and roughness. These procedures serve for concretely observe the behavior of these fields ans as a benchmark for the validation of anisotropy detection tools. We finally propose methods for estimating the anisotropy of a specific AFBF and for characterizing the probability distribution of orientation estimators.

Key words. local orientation, local Hurst index, anisotropic self-similar Gaussian fields, tangent fields, turning bands, oriented textures, roughness, kriging

AMS subject classifications. 68U10, 60G15, 62M40, 60G18, 28A80, 60G22, 60H05, 28C20, 62J10, 65K05

1. Introduction.

Texture modeling is a challenging issue of image processing. There is a variety of texture methods in the field of computer vision, namely structural, statistical, model-based and transform-based methods [18, 51, 45, 12, 41, 47]. While it is difficult to give a strict mathematical definition of textures, most proposed methods tackle their analysis and synthesis using random fields. In many cases, the model has to incorporate some important characteristics of the data as roughness or anisotropy properties. Several examples can be found in image processing, hydrology, geostatistics and spatial statistics (see, for example, Davies and Hall [14], Bonami and Estrade [9], Benson et al. [6]). It gives rise to several models including both roughness and anisotropy properties as fractional Brownian sheet [24, 1], anisotropic fractional Brownian field (AFBF) [9] or [21, 6] using the fractal framework. Typically, an AFBF has a harmonizable representation of the form

$$X(\boldsymbol{x}) = \int_{\mathbb{R}^2} \left(\mathrm{e}^{\mathrm{j}\langle \boldsymbol{x}, \boldsymbol{\xi} \rangle} - 1 \right) f(\boldsymbol{\xi})^{1/2} \, \widehat{\mathbf{W}}(\mathrm{d}\boldsymbol{\xi}) \, , \tag{1.1}$$

where f is the density function carrying the anisotropy property. The AFBF are fields with stationary increments. Stationary models have been especially of interest after Julesz's conjecture [22], which states that humans cannot distinguish between textures with identical second-order statistics. This conjecture has proved to be false in the general case [23]. Others models of anisotropic textures called locally parallel textures,

*Part of this work has appeared in preliminary form in the conference proceedings of the *IEEE International Conference On Image Processing (ICIP 2014)*, 2014 [37].

†Univ. Grenoble Alpes, CNRS, Grenoble INP, LJK, F-38000, Grenoble, France (kevin.polisano@univ-grenoble-alpes.fr).

‡Univ. Grenoble Alpes, CNRS, Grenoble INP, GIPSA-lab, F-38000, Grenoble, France (laurent.condat@gipsa-lab.grenoble-inp.fr).

have also been recently introduced in [32]. The mathematical definition and computational synthesis of *locally* anisotropic textures is then an important issue, since it provides flexible models enabling to test estimation procedures of the anisotropic *local* characteristics of an image. It could be also a first step to test isotropy properties of an image as in [44] or [42]. Here we focus on anisotropic *local properties* of Gaussian textures and provide a new Gaussian model whose anisotropic and roughness properties are prescribed at every point, through a local density function $(\boldsymbol{x}, \boldsymbol{\xi}) \mapsto f(\boldsymbol{x}, \boldsymbol{\xi})$, whose harmonizable representation is

$$X(\boldsymbol{x}) = \int_{\mathbb{R}^2} \left(\mathrm{e}^{\mathrm{j}\langle \boldsymbol{x}, \boldsymbol{\xi} \rangle} - 1 \right) f(\boldsymbol{x}, \boldsymbol{\xi})^{1/2} \, \widehat{\mathbf{W}}(\mathrm{d}\boldsymbol{\xi}) \; . \tag{1.2}$$

It is a first preliminary and important step in defining new statistical estimators of the local anisotropic features of a given texture. As in the case of multifractional Brownian motion (see [35, 4] for a definition and [3, 1, 2] for a deep study of properties of MBM and some of its extensions in various framework) which extend usual fractional Brownian motion (FBM) in the sense that the tangent fields of MBM are FBM, our model is an extension of anisotropic fractional Brownian field (AFBF) defined [9] in the sense that at each point its tangent fields is a AFBF. Since efficient methods as turning bands [7] have been developed for simulation of AFBF, we can provide efficient ways of synthesize the model.

The paper is organized as follows. In section 2 we briefly review some definitions. We also introduce our new model of locally self-similar Gaussian fields with prescribed local orientation, and give its main properties such as the tangent fields and covariance expressions needed for the further synthesis. In section 3 we define the notion of orientation for a large class of Gaussian fields called localizable fields, based on a Riesz-wavelet decomposition with an isotropic filter. In section 4, we use the results stated in section 2 to provide a synthesis method of our model based on turning bands. We also give an heuristic to simulate a more efficient simulation method in two steps for a subclass of the model where the local density is a cone and where the Hurst index is varying, thanks to the kriging method and the knowledge of the covariance. Then another model of deformation fields, more suited for texture synthesis with constant Hurst index, is provided in section 5. Finally, methods for detecting and characterizing orientations of a specific AFBF are developed in section 6.

2. A Gaussian locally-self model with prescribed local orientation.

2.1. Definitions. We recall below the definition of Generalized Anisotropic Fractional Brownian Fields (GAFBF) introduced in [39]. This general Gaussian field model is defined from two functions h from $\mathbb{R}^2$ to $[0,1]$ and C from $\mathbb{R}^2 \times \mathbb{R}^2$ to $\mathbb{R}_+$ satisfying the following set of assumptions:

Assumptions $(\mathcal{H})$

(i) h is a β–Hölder function, such that

$$a = \inf_{\boldsymbol{x} \in \mathbb{R}^2} h(\boldsymbol{x}) > 0, \quad b = \sup_{\boldsymbol{x} \in \mathbb{R}^2} h(\boldsymbol{x}) < \beta \leq 1 \; .$$

(ii) $(\boldsymbol{x}, \boldsymbol{\xi}) \mapsto C(\boldsymbol{x}, \boldsymbol{\xi})$ is bounded, that is

$$\forall (\boldsymbol{x}, \boldsymbol{\xi}) \in \mathbb{R}^2 \times \mathbb{R}^2, \quad C(\boldsymbol{x}, \boldsymbol{\xi}) \leqslant M \; .$$

(iii) $\boldsymbol{\xi} \mapsto C(\boldsymbol{x}, \boldsymbol{\xi})$ is even and homogeneous of degree 0:

$$\forall \rho > 0, \quad C(\boldsymbol{x}, \rho\boldsymbol{\xi}) = C(\boldsymbol{x}, \boldsymbol{\xi}) \; .$$

(iv) $\boldsymbol{x} \mapsto C(\boldsymbol{x}, \boldsymbol{\xi})$ is continuous and there exists some η, with $\beta \leq \eta \leq 1$ such that

$$\forall \boldsymbol{x} \in \mathbb{R}^2, \quad A_{\boldsymbol{x}} \stackrel{\text{def}}{=} \sup_{\boldsymbol{z} \in \mathbb{R}^2} \|\boldsymbol{z}\|^{-2\eta} \int_{\mathbb{S}^1} \left[C(\boldsymbol{x}+\boldsymbol{z}, \boldsymbol{\Theta}) - C(\boldsymbol{x}, \boldsymbol{\Theta})\right]^2 \mathrm{d}\boldsymbol{\Theta} < \infty \; . \tag{2.1}$$

Morever $\boldsymbol{x} \mapsto A_{\boldsymbol{x}}$ is bounded on any compact set of $\mathbb{R}^2$.
($\mathbb{S}^1$ denotes the unit circle, that is $\mathbb{S}^1 = \{\boldsymbol{\Theta} \in \mathbb{R}^2, \, \|\boldsymbol{\Theta}\| = 1\}$).

The definition of the GAFBF in the general framework (1.2) is then:

Definition 2.1 (Generalized Anisotropic Fractional Brownian Fields).
Let us consider $h : \mathbb{R}^2 \to [0,1]$ and C satisfying Assumptions $(\mathcal{H})$. We then define the Generalized Anisotropic Fractional Brownian Fields (GAFBF) by

$$X(\boldsymbol{x}) \stackrel{\text{def}}{=} \int_{\mathbb{R}^2} (\mathrm{e}^{\mathrm{j}\langle \boldsymbol{x}, \boldsymbol{\xi} \rangle} - 1) \frac{C(\boldsymbol{x}, \boldsymbol{\xi})}{\|\boldsymbol{\xi}\|^{h(\boldsymbol{x})+1}} \widehat{\mathbf{W}}(\mathrm{d}\boldsymbol{\xi}) \; . \tag{2.2}$$

Remark 2.2. Assumption (i) requiring that the Hölder coefficient β of X has to be greater than the supremum of h denoted by b, means that the function h which prescribes the local regularity $h(\boldsymbol{x})$ of X, cannot have a greater irregularity than the regularity of the field it governs. It is therefore a reasonable assumption, which is also made in the founding article of the multifractional Brownian motion [35, 4].

Remark 2.3. Now let us comment on the assumptions made about the function C which encodes the local anisotropy of the field X. Assumption (iii) requiring that C is even in $\boldsymbol{\xi}$ ensures that X is real and the degree homogeneity 0 simply means that for $\boldsymbol{x} \in \mathbb{R}^2$ fixed, if we know the function $\boldsymbol{\Theta} \mapsto C(\boldsymbol{x}, \boldsymbol{\Theta})$ on $\mathbb{S}^1$, then C is known for all frequencies since it is constant on the radial lines $\boldsymbol{\xi} = \rho\boldsymbol{\Theta}$, the anisotropy being a directional notion. Finally, the last assumption (iv) on C is stronger than continuity but weaker than hölderianity, since when $\boldsymbol{x} \mapsto C(\boldsymbol{x}, \boldsymbol{\xi})$ is η–Hölder (with a regularity at least equal to that of h since $\beta \leq \eta$), then it satisfies (2.1) with the same constant $A_{\boldsymbol{x}} \equiv A$ everywhere. We thus underline that the assumption $(\mathcal{H})$ are not restrictive and that the GAFBF model define a large class of Gaussian fields controlling local regularity and anisotropy.

We review hereafter few examples of such fields:

- For $h \equiv H$ and $C \equiv 1$ we recover the Fractional Brownian Field (FBF) [28], which is the only isotropic Gaussian field self-similar with parameter H and with stationary increments (see Figure 1a, Figure 1b and Figure 1c).
- For $h \equiv h(\boldsymbol{x})$ and $C \equiv 1$ we recover the Multifractional Brownian Field (MBF) whose regularity governed by h can spatially varied [35, 4]. This field has no longer stationary increments and is locally asymptotically self-similar (see Figure 1d).
- For $h \equiv H$ and $C \equiv C(\boldsymbol{\xi}/\|\boldsymbol{\xi}\|)$ we obtain self-similar fields with parameter H and with stationary increments (H-sssi), for which results a global anisotropy [9, 7]. The function $\boldsymbol{\xi} \mapsto C(\boldsymbol{\xi}/\|\boldsymbol{\xi}\|)$ is called the *anisotropy* function.
  Example: The elementary fields
  When the anisotropy function $C(\boldsymbol{\xi}/\|\boldsymbol{\xi}\|) = c_{\theta_1,\theta_2}(\arg \boldsymbol{\xi})$ is a cone, that is

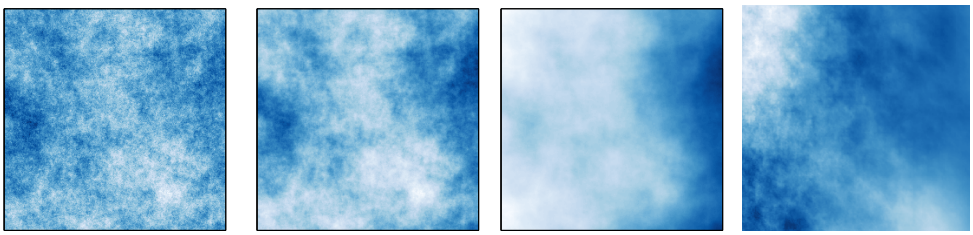

(a) $H = 0.2$ (b) $H = 0.5$ (c) $H = 0.8$ (d) $h(\boldsymbol{x}) = 0.5 + 0.4x_1$

Fig. 1: (a)-(c) Fractional Brownian Fields (FBF) for different Hurst index and (d) a Multifractional Brownian Field (MBM) for a Hurst function varying horizontally.

$c_{\theta_1,\theta_2} : \theta \mapsto \mathbb{1}_{[\theta_1,\theta_2]}(\theta)$ is a π-periodic function defined on $(-\pi/2, \pi/2]$, we specifically obtain a H-sssi field called *elementary field* in the terminology of [7], whose harmonizable representation is:

$$Y_{H,\theta_1,\theta_2}(\boldsymbol{x}) \stackrel{\text{def}}{=} \int_{\mathbb{R}^2} \left(\mathrm{e}^{\mathrm{j}\langle \boldsymbol{x},\, \boldsymbol{\xi}\rangle} - 1\right) \frac{c_{\theta_1,\theta_2}(\arg \boldsymbol{\xi})}{\|\boldsymbol{\xi}\|^{H+1}} \widehat{\mathbf{W}}(\mathrm{d}\boldsymbol{\xi}), \quad \forall \boldsymbol{x} \in \mathbb{R}^2 \,. \tag{2.3}$$

These elementary fields produce globally oriented textures in the direction perpendicular to $\alpha_0 = \frac{1}{2}(\theta_1 + \theta_2)$, whose degree of directionality is controlled by the half-width of the cone $\delta = |\theta_1 - \theta_2|/2$, as illustrated in Figure 2.

- For $h \equiv H$ and $C \equiv C(\boldsymbol{x}, \boldsymbol{\xi})$ we proposed in [37, 38] a local version of these *elementary fields* for which results a texture locally oriented (see Figure 3).
- For $h \equiv h(\boldsymbol{x})$ and $C \equiv C(\boldsymbol{x}, \boldsymbol{\xi})$, we extend in this paper the previous case by taking into account local orientation and local roughness both. The corresponding Gaussian field, called Locally Anisotropic Fractional Brownian Field (LAFBF), is presented in Definition 2.6 and will be simulated in section 4.

Remark 2.4. Let us note that the usual models such as the fractional Brownian field (FBF) or the multifractional Brownian field (MBF), are respectively normalized by a constant C_H and a function $C_{h(\boldsymbol{x})}$, where

$$C_H = \frac{\pi^{3/2}\Gamma\left(H + \frac{1}{2}\right)}{H\Gamma(2H)\sin(H\pi)\Gamma\left(H+1\right)} \,, \tag{2.4}$$

so that the variance of the field is equal to 1 on the unit sphere, *i.e* $\mathrm{Var}[X(\boldsymbol{x})] = 1$, for all $\boldsymbol{x} \in \mathbb{S}^1$. We must therefore ensure that such a normalization does not contravene the condition (2.1), hence the preliminary lemma that follows.

LEMMA 2.5. *Let $\widetilde{C} : (\boldsymbol{x}, \boldsymbol{\xi}) \mapsto \widetilde{C}(\boldsymbol{x}, \boldsymbol{\xi})$ be a local anisotropy function satisfying assumptions $(\mathcal{H})$, so that in particular the condition (2.1). We define a normalized function $N : \boldsymbol{x} \mapsto N(\boldsymbol{x})$, supposed to be C^1 and bounded. Then, the normalized local anisotropy function C defined by:*

$$C(\boldsymbol{x}, \boldsymbol{\xi}) = \frac{\widetilde{C}(\boldsymbol{x}, \boldsymbol{\xi})}{N(\boldsymbol{x})} \,, \tag{2.5}$$

also satisfies assumptions $(\mathcal{H})$ and in particular (2.1).

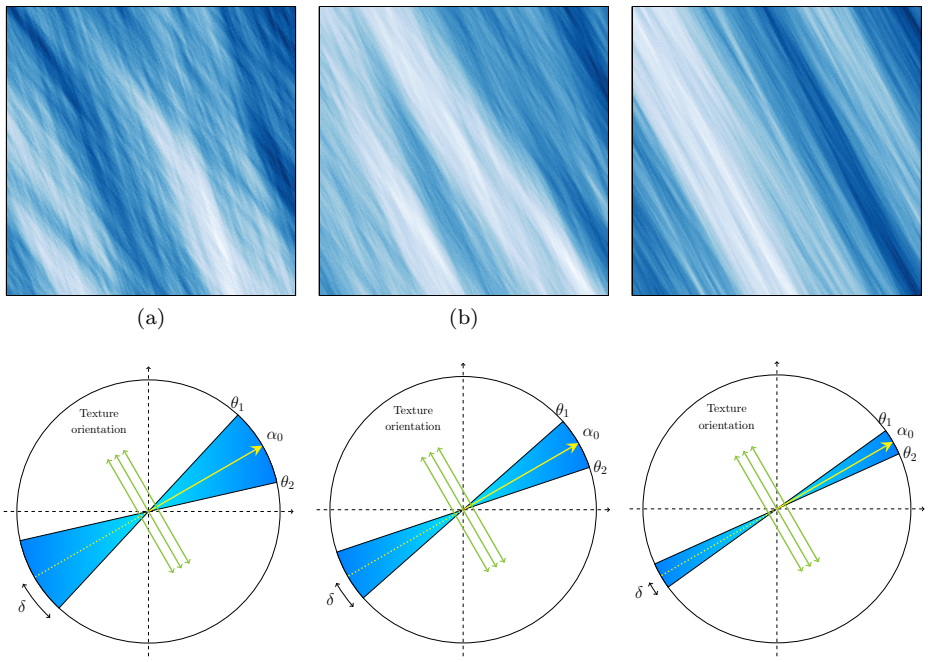

Fig. 2: Simulation of an elementary field of size $r = 255$, $\alpha_0 = \pi/6$, $H = 0.5$ and different half-width of the cone (a)-(d) $\delta = 3.10^{-1}$, (b)-(e) $\delta = 2.10^{-1}$ et (c)-(f) $\delta = 1.10^{-1}$.

Proof. Showing that C satisfies assumptions (ii) and (iii) is straightforward. Let us examine assumption (iv). Let us take $\boldsymbol{x} \in \mathbb{R}^2$ and $\boldsymbol{z} \in B(\mathbf{0}, 1)$. Since $\widetilde{C}$ is bounded by $M_{\widetilde{C}}$ and N is supposed to be C^1 and bounded on $\mathbb{R}^2$ in a range $[m_N, M_N]$, we have

$$\begin{aligned}
\left|C(\boldsymbol{x}+\boldsymbol{z},\cdot) - C(\boldsymbol{x},\cdot)\right| &= \left|\frac{\widetilde{C}(\boldsymbol{x}+\boldsymbol{z},\cdot)}{N(\boldsymbol{x}+\boldsymbol{z})} - \frac{\widetilde{C}(\boldsymbol{x},\cdot)}{N(\boldsymbol{x})}\right| , \\
&= \left|\frac{(\widetilde{C}(\boldsymbol{x}+\boldsymbol{z},\cdot) - \widetilde{C}(\boldsymbol{x},\cdot))N(\boldsymbol{x}) + \big(N(\boldsymbol{x}+\boldsymbol{z}) - N(\boldsymbol{x})\big)\,\widetilde{C}(\boldsymbol{x},\cdot)}{N(\boldsymbol{x}+\boldsymbol{z})N(\boldsymbol{x})}\right| , \\
&\leq \frac{\left|\widetilde{C}(\boldsymbol{x}+\boldsymbol{z},\cdot) - \widetilde{C}(\boldsymbol{x},\cdot)\right| M_N + \left|N(\boldsymbol{x}+\boldsymbol{z}) - N(\boldsymbol{x})\right| M_{\widetilde{C}}}{m_N^2} .
\end{aligned}$$

By integrating, and using the inequality $(a+b)^2 \leq 2(a^2+b^2)$, we get

$$\begin{aligned}
&\|\boldsymbol{z}\|^{-2\eta} \int_{\mathbb{S}^1} \left|C(\boldsymbol{x}+\boldsymbol{z},\boldsymbol{\Theta}) - C(\boldsymbol{x},\boldsymbol{\Theta})\right|^2 \mathrm{d}\boldsymbol{\Theta} \\
&\leq \frac{2M_N^2}{m_N^4}\|\boldsymbol{z}\|^{-2\eta} \int_{\mathbb{S}^1} \left|\widetilde{C}(\boldsymbol{x}+\boldsymbol{z},\boldsymbol{\Theta}) - \widetilde{C}(\boldsymbol{x},\boldsymbol{\Theta})\right|^2 \mathrm{d}\boldsymbol{\Theta} , \\
&\quad + \frac{4\pi M_{\widetilde{C}}^2}{m_N^4}\|\boldsymbol{z}\|^{-2\eta}\left|N(\boldsymbol{x}+\boldsymbol{z}) - N(\boldsymbol{x})\right|^2 .
\end{aligned}$$

N is C^1, so by the mean value inequality:

$$\|\boldsymbol{z}\|^{-2\eta}\big|N(\boldsymbol{x}+\boldsymbol{z})-N(\boldsymbol{x})\big|^2 \leq \Lambda_{\boldsymbol{x}}^2\|\boldsymbol{z}\|^{2-2\eta} \leq \Lambda_{\boldsymbol{x}}^2 \ ,$$

since $\boldsymbol{z} \in B(\mathbf{0},1)$ and $0 \leq \eta \leq 1$. Moreover $\boldsymbol{x} \mapsto \Lambda_{\boldsymbol{x}}$ is bounded on every compact since N is C^1. By assumption $\widetilde{C}$ satisfies (2.1), then we have for all $\boldsymbol{x} \in \mathbb{R}^2$

(2.6)
$$\sup_{\boldsymbol{z}\in B(\mathbf{0},1)} \|\boldsymbol{z}\|^{-2\eta} \int_{\mathbb{S}^1} \big[C(\boldsymbol{x}+\boldsymbol{z},\boldsymbol{\Theta})-C(\boldsymbol{x},\boldsymbol{\Theta})\big]^2 \,\mathrm{d}\boldsymbol{\Theta} \leq \underbrace{\frac{2M_N^2}{m_N^4}\widetilde{A}_{\boldsymbol{x}} + \frac{4\pi M_{\widetilde{C}}^2}{m_N^4}\Lambda_{\boldsymbol{x}}^2}_{A_{\boldsymbol{x}}} < \infty \ .$$

and $A_{\boldsymbol{x}}$ is bounded on every compact since $\widetilde{A}_{\boldsymbol{x}}$ and $\Lambda_{\boldsymbol{x}}^2$ are bounded on every compact□

Definition 2.6 (Locally Anisotropic Fractional Brownian Field). *Let $h : \mathbb{R}^2 \to [0,1]$ be a β–Hölder function satisfying $a = \inf_{\boldsymbol{x}\in\mathbb{R}^2} h(\boldsymbol{x}) > 0$ and $b = \sup_{\boldsymbol{x}\in\mathbb{R}^2} h(\boldsymbol{x}) < \beta \leq \eta \leq 1/2$; and let α, δ two 2η–Hölder functions defined from $\mathbb{R}^2$ to $\mathbb{R}$. In addition, we assume that $0 < \inf_{\boldsymbol{x}\in\mathbb{R}^2} \delta(\boldsymbol{x}) \leq \sup_{\boldsymbol{x}\in\mathbb{R}^2} \delta(\boldsymbol{x}) < \pi$. We define the Locally Anisotropic Fractional Brownian Field (LAFBF) $B^h_{\alpha,\delta}$ with Hurst function h, orientation function α and directionality function δ, by the following harmonizable representation:*

$$B^h_{\alpha,\delta}(\boldsymbol{x}) \stackrel{\text{def}}{=} \frac{1}{C^h_{\alpha,\delta}(\boldsymbol{x})} \int_{\mathbb{R}^2} \left(\mathrm{e}^{\mathrm{j}\langle \boldsymbol{x},\boldsymbol{\xi}\rangle} - 1\right) \frac{c_{\alpha,\delta}(\boldsymbol{x},\arg\boldsymbol{\xi})}{\|\boldsymbol{\xi}\|^{h(\boldsymbol{x})+1}} \widehat{\mathbf{W}}(\mathrm{d}\boldsymbol{\xi}) \ . \tag{2.7}$$

with the local anisotropy function

$$c_{\alpha,\delta}(\boldsymbol{x},\cdot) = c_{\alpha(\boldsymbol{x})-\delta(\boldsymbol{x}),\alpha(\boldsymbol{x})+\delta(\boldsymbol{x})} \ , \tag{2.8}$$

where the π–periodic function $\theta \mapsto c_{\theta_1,\theta_2}(\theta)$ is defined on $(-\pi/2,\pi/2]$ by:

$$c_{\theta_1,\theta_2}(\theta) = \mathbb{1}_{[\theta_1,\theta_2]}(\theta), \quad \theta \in (-\pi/2,\pi/2], \quad \boldsymbol{x} \in \mathbb{R}^2 \ , \tag{2.9}$$

and where $C^h_{\alpha,\delta}(\boldsymbol{x})$ is a C^1 normalized function, which is bounded and will be explicitly defined in (2.25).

Remark 2.7. The local anisotropy function $c_{\alpha,\delta}(\boldsymbol{x},\cdot)$ is the *localized version* of the elementary field's anisotropy function. Thus, $c_{\alpha,\delta}(\boldsymbol{x},\cdot)$ can be viewed as a cone, where α and δ are now functions which govern spatially the orientation and the directionality in every $\boldsymbol{x} \in \mathbb{R}^2$, as illustrated in Figure 3 for $h \equiv H$ constant, corresponding to the definition introduced in [37]. Intuitively, the smaller $\delta(\boldsymbol{x})$ is, the more the texture will be sharply oriented in the direction $\alpha(\boldsymbol{x})$ on the neighborhood of a point $\boldsymbol{x} \in \mathbb{R}^2$. We will precise the notion of orientation of a Gaussian field in section 3. In this extended definition, the Hurst function h is an indicator of the texture roughness which can now vary spatially. The restricted condition relating to the range of h can be relaxed using a C^∞-regularized version $\widetilde{c}_{\alpha,\delta}$ of the characteristic function.

Proposition 2.8. *The functions h and $C(\boldsymbol{x},\boldsymbol{\xi}) = \frac{c_{\alpha,\delta}(\boldsymbol{x},\arg\boldsymbol{\xi})}{C^h_{\alpha,\delta}(\boldsymbol{x})}$ in Definition 2.6 satisfy assumptions $(\mathcal{H})$, that is the LAFBF is a specific case of the GAFBF model.*

Proof. The function h clearly satisfies $(\mathcal{H})$, with the stronger constraint $\eta \leq 1/2$ (and then $\beta \leq 1/2$). Since $C^h_{\alpha,\delta}$ is supposed to be C^1 and bounded on $\mathbb{R}^2$, then according to Lemma 2.5 it is sufficient to prove that

$$\forall \boldsymbol{x} \in \mathbb{R}^2, \quad \sup_{\boldsymbol{z}\in B(\mathbf{0},1)} \|\boldsymbol{z}\|^{-2\eta} \int_{\mathbb{S}^1} \left[\widetilde{C}(\boldsymbol{x}+\boldsymbol{z},\boldsymbol{\Theta}) - \widetilde{C}(\boldsymbol{x},\boldsymbol{\Theta})\right]^2 \mathrm{d}\boldsymbol{\Theta} \leq A_{\boldsymbol{x}} < \infty \ , \tag{2.10}$$

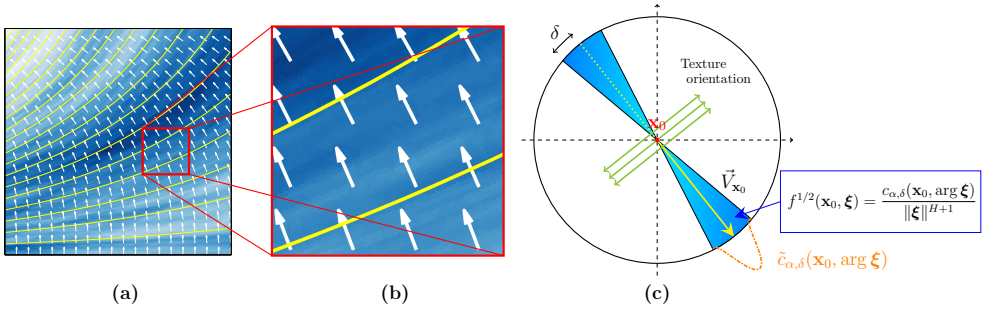

Fig. 3: (a) LAFBF synthesis in every point $\boldsymbol{x} = (x_1, x_2)$, the resulting texture is oriented according to the vector field $\boldsymbol{V}(x_1, x_2) = (-\sin\alpha(x_1, x_2), \cos\alpha(x_1, x_2))$ with $\alpha(x_1, x_2) = -\frac{\pi}{2} + x_1$, $\delta = 3.10^{-2}$ and $H = 0.8$ constants, (b) zoom around a point $\boldsymbol{x}_0$ illustrating that the LAFBF behaves locally as an elementary field, (c) a diagram illustrating the role played by parameters α and δ in a neighborhood of a point $\boldsymbol{x}_0$, respectively encoding the local orientation of the texture (governed by the cone's direction) and its directionality (governed by the cone's half-width).

where

$$\widetilde{C}(\boldsymbol{x}, \boldsymbol{\xi}) = c_{\alpha,\delta}(\boldsymbol{x}, \arg\boldsymbol{\xi}) = c_{\alpha(\boldsymbol{x})-\delta(\boldsymbol{x}),\alpha(\boldsymbol{x})+\delta(\boldsymbol{x})}(\arg\boldsymbol{\xi}) \; .$$

Let us fix $\boldsymbol{x} \in \mathbb{R}^2$. Since α and δ are continuous, there exists $\nu > 0$ such that for $\|\boldsymbol{z}\| < \nu$ the cones $\widetilde{C}(\boldsymbol{x}+\boldsymbol{z}, \cdot)$ and $\widetilde{C}(\boldsymbol{x}, \cdot)$ intersect each other. We then distinguish two cases:

- If there exists $\boldsymbol{z} \in \mathcal{B}(\boldsymbol{0}, \nu)^c$ such that the functions $\widetilde{C}(\boldsymbol{x}, \cdot)$ and $\widetilde{C}(\boldsymbol{x}+\boldsymbol{z}, \cdot)$ have disjointed supports, then the quantity (2.10) is computed from:

$$\begin{aligned}\int_{\mathbb{S}^1} \widetilde{C}(\boldsymbol{x}+\boldsymbol{z}, \boldsymbol{\Theta})^2 \, \mathrm{d}\boldsymbol{\Theta} = \quad & 2\int_0^{2\pi} \mathbb{1}_{\alpha(\boldsymbol{x}+\boldsymbol{z})-\delta(\boldsymbol{x}+\boldsymbol{z}),\alpha(\boldsymbol{x}+\boldsymbol{z})+\delta(\boldsymbol{x}+\boldsymbol{z})}(\theta) \, \mathrm{d}\theta \; , \\ = \quad & 4\delta(\boldsymbol{x}+\boldsymbol{z}) \; .\end{aligned}$$

$$\begin{aligned}\int_{\mathbb{S}^1} \widetilde{C}(\boldsymbol{x}, \boldsymbol{\Theta})^2 \, \mathrm{d}\boldsymbol{\Theta} = \quad & 2\int_0^{2\pi} \mathbb{1}_{\alpha(\boldsymbol{x})-\delta(\boldsymbol{x}),\alpha(\boldsymbol{x})+\delta(\boldsymbol{x})}(\theta) \, \mathrm{d}\theta \; , \\ = \quad & 4\delta(\boldsymbol{x}) \; .\end{aligned}$$

  Hence

$$\|\boldsymbol{z}\|^{-2\eta} \int_{\mathbb{S}^1} \left[\widetilde{C}(\boldsymbol{x}+\boldsymbol{z}, \boldsymbol{\Theta}) - \widetilde{C}(\boldsymbol{x}, \boldsymbol{\Theta})\right]^2 \mathrm{d}\boldsymbol{\Theta} \leq \frac{8 \sup_{\boldsymbol{x}\in\mathbb{R}^2} \delta(\boldsymbol{x})}{\|\boldsymbol{z}\|^{2\eta}} \leq \frac{8\pi}{\nu^{2\eta}} < \infty \; .$$

- Else if $\boldsymbol{z} \in \mathcal{B}(\boldsymbol{0}, \nu)$, then we have to withdraw the intersection:

$$\begin{aligned}&\int_0^{2\pi} \mathbb{1}_{\alpha(\boldsymbol{x}+\boldsymbol{z})-\delta(\boldsymbol{x}+\boldsymbol{z}),\alpha(\boldsymbol{x}+\boldsymbol{z})+\delta(\boldsymbol{x}+\boldsymbol{z})}(\theta) \mathbb{1}_{\alpha(\boldsymbol{x})-\delta(\boldsymbol{x}),\alpha(\boldsymbol{x})+\delta(\boldsymbol{x})}(\theta) \, \mathrm{d}\theta \\ &= \int_0^{2\pi} \mathbb{1}_{\max(\alpha(\boldsymbol{x}+\boldsymbol{z})-\delta(\boldsymbol{x}+\boldsymbol{z}),\alpha(\boldsymbol{x})-\delta(\boldsymbol{x})),\min(\alpha(\boldsymbol{x}+\boldsymbol{z})+\delta(\boldsymbol{x}+\boldsymbol{z}),\alpha(\boldsymbol{x})+\delta(\boldsymbol{x}))}(\theta) \, \mathrm{d}\theta \; , \\ &= \min(\alpha(\boldsymbol{x}+\boldsymbol{z}) + \delta(\boldsymbol{x}+\boldsymbol{z}), \alpha(\boldsymbol{x}) + \delta(\boldsymbol{x})) \\ &\quad - \max(\alpha(\boldsymbol{x}+\boldsymbol{z}) - \delta(\boldsymbol{x}+\boldsymbol{z}), \alpha(\boldsymbol{x}) - \delta(\boldsymbol{x})) \; ,\end{aligned}$$

and using the relations $\max(a,b) = \frac{a+b+|a-b|}{2}$ and $\min(a,b) = \frac{a+b-|a-b|}{2}$ we obtain

$$\|\boldsymbol{z}\|^{-2\eta} \int_{\mathbb{S}^1} \left[\widetilde{C}(\boldsymbol{x}+\boldsymbol{z},\boldsymbol{\Theta}) - \widetilde{C}(\boldsymbol{x},\boldsymbol{\Theta})\right]^2 \mathrm{d}\boldsymbol{\Theta} \,, \tag{2.11}$$
$$= 2 \cdot \frac{\left|\alpha_-(\boldsymbol{x}+\boldsymbol{z}) - \alpha_-(\boldsymbol{x})\right| + \left|\alpha_+(\boldsymbol{x}+\boldsymbol{z}) - \alpha_+(\boldsymbol{x})\right|}{\|\boldsymbol{z}\|^{2\eta}} \,,$$

with $\alpha_-(\boldsymbol{x}) = \alpha(\boldsymbol{x}) - \delta(\boldsymbol{x})$ and $\alpha_+(\boldsymbol{x}) = \alpha(\boldsymbol{x}) + \delta(\boldsymbol{x})$. Finally, since α and δ are 2η–Hölder functions with $\eta \leq 1/2$, then α_- and α_+ are too, therefore the supremum of the quantity Proof 2 on all $\boldsymbol{z} \in B(\mathbf{0},1)$ is finite, which concludes the proof. ∎

2.2. Properties of the GAFBF and LAFBF. The simulation of the GAFBF or LAFBF and the definition of the local orientations require to describe the random field locally. To this purpose we need the notion of tangent fields. This enables to link GAFBF with H-sssi fields, and in particular LAFBF with elementary fields, viewed as a local version of the latter. Then, we both explicit the covariance characterizing the elementary fields and further the LAFBF, which is useful for the exact simulation of this field.

2.2.1. Tangent field. We now introduce the notion of tangent fields. We first recall, following [5, 16, 17], the definition of H–localizable Gaussian fields.

DEFINITION 2.9 (Localizable Gaussian field). *Let $H \in (0,1)$. We say that the random field $X = \{X(\boldsymbol{x}),\, \boldsymbol{x} \in \mathbb{R}^2\}$ is H–localizable at $\boldsymbol{x_0} \in \mathbb{R}^2$ with tangent field (or local form) the random field $Y_{\boldsymbol{x_0}} = \{Y_{\boldsymbol{x_0}}(\boldsymbol{x}),\, \boldsymbol{x} \in \mathbb{R}^2\}$ if*

$$\left\{ \frac{X(\boldsymbol{x_0}+\rho\boldsymbol{x}) - X(\boldsymbol{x_0})}{\rho^H} \right\}_{\boldsymbol{x}\in\mathbb{R}^2} \xrightarrow{d} \left\{Y_{\boldsymbol{x_0}}(\boldsymbol{x})\right\}_{\boldsymbol{x}\in\mathbb{R}^2} \,, \tag{2.12}$$

as $\rho \to 0$, where $\xrightarrow{d}$ means convergence in distribution, that is the weak convergence for stochastic processes (see [8]). A random field $X = \{X(\boldsymbol{x}),\, \boldsymbol{x} \in \mathbb{R}^2\}$ is said to be localizable if for all $\boldsymbol{x} \in \mathbb{R}^2$ it is H–localizable for some $H \in (0,1)$.

In Theorem 3.9 and Corollary 3.10 of [16], Falconer proved the following result that we state in the Gaussian case. It enables to describe the whole class of possible tangent fields of a Gaussian field with continuous sample paths.

THEOREM 2.10. *Let X be a localizable Gaussian field with continuous sample paths. For almost all $\boldsymbol{x_0}$ in $\mathbb{R}^2$ the tangent field $Y_{\boldsymbol{x_0}}$ of X at $\boldsymbol{x_0}$ has stationary increments and is self-similar, that is for some $H \in (0,1)$ and for all $\rho \geq 0$,*

$$\{Y_{\boldsymbol{x_0}}(\rho\boldsymbol{x}),\, \boldsymbol{x} \in \mathbb{R}^2\} \overset{(fdd)}{=} \{\rho^H Y_{\boldsymbol{x_0}}(\boldsymbol{x}),\, \boldsymbol{x} \in \mathbb{R}^2\} \,. \tag{2.13}$$

In short, a Gaussian field with continuous sample paths will have at a.e. point, a "fractal" tangent field behaving like a FBF. Roughly speaking, the random field X admits the tangent field $Y_{\boldsymbol{x_0}}$ at a given point $\boldsymbol{x_0}$ if it behaves locally as $Y_{\boldsymbol{x_0}}$ when $\boldsymbol{x} \to \boldsymbol{x_0}$. This notion has been first introduced in [4] to describe the local behavior of Multifractional Brownian Motion (which behaves locally as a FBM).

We now illustrate this notion considering a classical example of Gaussian field with prescribed tangent field: the Multifractional Brownian Field defined in the unidimensional setting in [27], and in the multivariate case in [5, 20].

Example: The Multifractional Brownian Field (MBF)
Let $h : \mathbb{R}^2 \to (0,1)$ be a continuously differentiable function whose range is supposed to be a compact interval $[a,b] \subset (0,1)$. The Multifractional Brownian Field with multifractional function h, is the Gaussian field defined by its harmonisable representation as follows

$$X_h(\boldsymbol{x}) = \int_{\mathbb{R}^2} \frac{\mathrm{e}^{\mathrm{j}\langle \boldsymbol{x},\, \boldsymbol{\xi}\rangle} - 1}{\|\boldsymbol{\xi}\|^{h(\boldsymbol{x})+1}} \,\mathrm{d}\widehat{\mathbf{W}}(\boldsymbol{\xi}) \,. \tag{2.14}$$

The tangent field $Y_{\boldsymbol{x_0}}$ of the MBF X_h at point $\boldsymbol{x_0}$ is a FBF of order $h(\boldsymbol{x}_0)$.

In the following proposition, we provide an explicit expression of the tangent field of a GAFBF and LAFBF at any point.

Proposition 2.11. *The Gaussian field X defined by the harmonisable representation (2.2) admits a H-sssi tangent field $Y_{\boldsymbol{x_0}}$ at any point $\boldsymbol{x_0} \in \mathbb{R}^2$ defined as*

$$Y_{\boldsymbol{x_0}}(\boldsymbol{x}) = \int_{\mathbb{R}^2} (\mathrm{e}^{\mathrm{j}\langle \boldsymbol{x},\, \boldsymbol{\xi}\rangle} - 1) f^{1/2}(\boldsymbol{x_0}, \boldsymbol{\xi}) \widehat{\mathbf{W}}(\mathrm{d}\boldsymbol{\xi}) = \int_{\mathbb{R}^2} (\mathrm{e}^{\mathrm{j}\langle \boldsymbol{x},\, \boldsymbol{\xi}\rangle} - 1) \frac{C(\boldsymbol{x_0}, \boldsymbol{\xi})}{\|\boldsymbol{\xi}\|^{h(\boldsymbol{x_0})+1}} \widehat{\mathbf{W}}(\mathrm{d}\boldsymbol{\xi}) \,. \tag{2.15}$$

In particular, the LAFBF $B^h_{\alpha,\delta}$ (2.7) with Hurst function h, orientation function α and directionality function δ admits at any point $\boldsymbol{x_0} \in \mathbb{R}^2$ the tangent field

$$Y_{\boldsymbol{x}_0}(\boldsymbol{x}) = \frac{1}{C^h_{\alpha,\delta}(\boldsymbol{x}_0)} \int_{\mathbb{R}^2} \left(\mathrm{e}^{\mathrm{j}\langle \boldsymbol{x},\, \boldsymbol{\xi}\rangle} - 1\right) \frac{c_{\alpha(\boldsymbol{x}_0)-\delta(\boldsymbol{x}_0),\alpha(\boldsymbol{x}_0)+\delta(\boldsymbol{x}_0)}(\arg\, \boldsymbol{\xi})}{\|\boldsymbol{\xi}\|^{h(\boldsymbol{x}_0)+1}} \widehat{\mathbf{W}}(\mathrm{d}\boldsymbol{\xi}) \,, \tag{2.16}$$

which corresponds to an elementary field Y_{H,θ_1,θ_2} (2.3) where $H = h(\boldsymbol{x}_0)$, $\theta_1 = \alpha(\boldsymbol{x}_0) - \delta(\boldsymbol{x}_0)$ and $\theta_2 = \alpha(\boldsymbol{x}_0) + \delta(\boldsymbol{x}_0)$. Locally the LAFBF behaves like an elementary field.

Proof. The proof was given in our previous paper [39, Proposition 9]. ∎

2.2.2. Covariance. A Gaussian random field is completely characterized by its mean and covariance function. Moreover, we have the following result:

Proposition 2.12 (Semi-variogram). *A Gaussian random fields with stationary increments X is completely characterized by its variogram (or semi-variogram) v_X defined by:*

$$\forall \boldsymbol{y} \in \mathbb{R}^2, \quad v_X(\boldsymbol{y}) = \frac{1}{2}\mathbb{E}\left[(X(\boldsymbol{y}) - X(\mathbf{0}))^2\right] \,, \tag{2.17}$$

since the covariance is related to the variogram as follows:

$$\forall \boldsymbol{y}, \boldsymbol{z} \in \mathbb{R}^2, \quad \mathrm{Cov}(X(\boldsymbol{y}) - X(\mathbf{0}), X(\boldsymbol{z}) - X(\mathbf{0})) = v_X(\boldsymbol{y}) + v_X(\boldsymbol{z}) - v_X(\boldsymbol{y} - \boldsymbol{z}) \,.$$

Proof. Since X has stationary increments, we have equally variance of increments with same size:

$$\begin{aligned} v_X(\boldsymbol{y} - \boldsymbol{z}) &= \frac{1}{2}\mathbb{E}\left[(X(\boldsymbol{y} - \boldsymbol{z}) - X(\mathbf{0}))^2\right] = \frac{1}{2}\mathbb{E}\left[(X(\boldsymbol{y}) - X(\boldsymbol{z}))^2\right] \,, \\ &= \frac{1}{2}\mathbb{E}\left[X(\boldsymbol{y})^2\right] + \frac{1}{2}\mathbb{E}\left[X(\boldsymbol{z})^2\right] - \mathbb{E}\left[X(\boldsymbol{y})X(\boldsymbol{z})\right] \,. \end{aligned}$$

Besides,

$$v_X(\boldsymbol{y}) = \frac{1}{2}\mathbb{E}\left[X(\boldsymbol{y})^2\right] + \frac{1}{2}\mathbb{E}\left[X(\mathbf{0})^2\right] - \mathbb{E}\left[X(\boldsymbol{y})X(\mathbf{0})\right] \,, \tag{2.18}$$

$$v_X(\boldsymbol{z}) = \frac{1}{2}\mathbb{E}\left[X(\boldsymbol{z})^2\right] + \frac{1}{2}\mathbb{E}\left[X(\mathbf{0})^2\right] - \mathbb{E}\left[X(\boldsymbol{z})X(\mathbf{0})\right] \,, \tag{2.19}$$

∎

so that

$$\begin{aligned} & v_X(\boldsymbol{y}) + v_X(\boldsymbol{z}) - v_X(\boldsymbol{y}-\boldsymbol{z}) \\ &= \mathbb{E}\left[X(\boldsymbol{y})X(\boldsymbol{z})\right] + \mathbb{E}\left[X(\mathbf{0})^2\right] - \mathbb{E}\left[X(\boldsymbol{y})X(\mathbf{0})\right] - \mathbb{E}\left[X(\boldsymbol{z})X(\mathbf{0})\right] \ , \\ &= \mathrm{Cov}(X(\boldsymbol{y}) - X(\mathbf{0}), X(\boldsymbol{z}) - X(\mathbf{0})) \ . \end{aligned}$$

We observed in Proposition 2.11 that at each point $\boldsymbol{x_0}$, the tangent field $Y_{\boldsymbol{x_0}}$ of a LAFBF $B^h_{\alpha,\delta}$ is no more and no less than an elementary field Y_{H,θ_1,θ_2} defined in (2.3), which is a particular case of H-sssi fields that is with stationary increments. Then from Proposition 2.12 the elementary field Y_{H,θ_1,θ_2} is completely characterized by its variogram, whose expression can be explicitly computed as follows:

PROPOSITION 2.13. *The semi-variogram of Y_{H,θ_1,θ_2} is given by*

$$\forall \boldsymbol{x} \in \mathbb{R}^2, \quad v_{H,\theta_1,\theta_2}(\boldsymbol{x}) = 2^{2H-1}\gamma(H) C_{H,\theta_1,\theta_2}(\arg \boldsymbol{x}) \|\boldsymbol{x}\|^{2H} \ , \tag{2.20}$$

where C_{H,θ_1,θ_2} is a π-periodic function defined on $(-\pi/2, \pi/2]$ by

$$C_{H,\theta_1,\theta_2}(\theta) = \begin{cases} \beta_H\left(\frac{1-\sin(\theta_2-\theta)}{2}\right) + \beta_H\left(\frac{1-\sin(\theta_1-\theta)}{2}\right), & \text{if } \theta_1 \leqslant \theta + \pi/2 \leqslant \theta_2 \\ \beta_H\left(\frac{1+\sin(\theta_2-\theta)}{2}\right) + \beta_H\left(\frac{1+\sin(\theta_1-\theta)}{2}\right), & \text{if } \theta_1 \leqslant \theta - \pi/2 \leqslant \theta_2 \\ \left|\beta_H\left(\frac{1-\sin(\theta_2-\theta)}{2}\right) - \beta_H\left(\frac{1-\sin(\theta_1-\theta)}{2}\right)\right|, & \text{otherwise} \end{cases} , \tag{2.21}$$

and β_H is the incomplete Beta function defined by

$$\forall t \in [0,1], \quad \beta_H(t) = \int_0^t u^{H-1/2}(1-u)^{H-1/2} \ ,$$

and

$$\gamma(H) = \frac{\pi}{H\Gamma(2H)\sin(H\pi)} \ . \tag{2.22}$$

Proof. The proof is given in the supplementary material of [7]. ∎

PROPOSITION 2.14. *The covariance of the elementary field Y_{H,θ_1,θ_2} defined in (2.3) and denoted by r_{H,θ_1,θ_2} have from Proposition 2.12 the following expression:*

$$\begin{aligned} \forall \boldsymbol{x}, \boldsymbol{y} \in \mathbb{R}^2, \quad r_{H,\theta_1,\theta_2}(\boldsymbol{x},\boldsymbol{y}) &\overset{\text{def}}{=} \mathrm{Cov}\left(Y_{H,\theta_1,\theta_2}(\boldsymbol{x}), Y_{H,\theta_1,\theta_2}(\boldsymbol{y})\right) \ , \\ &= v_{H,\theta_1,\theta_2}(\boldsymbol{x}) + v_{H,\theta_1,\theta_2}(\boldsymbol{y}) - v_{H,\theta_1,\theta_2}(\boldsymbol{x}-\boldsymbol{y}) \ . \end{aligned} \tag{2.23}$$

We are now able to give an explicit formula for the covariance of a LAFBF. We have established the following result:

PROPOSITION 2.15. *The covariance of a LAFBF $B^h_{\alpha,\delta}(\boldsymbol{x})$ (2.7), with functions $\theta_1(\boldsymbol{x}) = \alpha(\boldsymbol{x}) - \delta(\boldsymbol{x})$ and $\theta_2(\boldsymbol{x}) = \alpha(\boldsymbol{x}) + \delta(\boldsymbol{x})$, is given for all $\boldsymbol{x}, \boldsymbol{y} \in \mathbb{R}^2$ by:*

$$\begin{aligned} & \mathrm{Cov}\left(B^h_{\alpha,\delta}(\boldsymbol{x}), B^h_{\alpha,\delta}(\boldsymbol{y})\right) \\ &= \frac{1}{C^h_{\alpha,\delta}(\boldsymbol{x}) C^h_{\alpha,\delta}(\boldsymbol{y})} \, r_{(h(\boldsymbol{x})+h(\boldsymbol{y}))/2, \max(\theta_1(\boldsymbol{x}),\theta_1(\boldsymbol{y})), \min(\theta_2(\boldsymbol{x}),\theta_2(\boldsymbol{y}))}(\boldsymbol{x},\boldsymbol{y}) \ , \end{aligned} \tag{2.24}$$

where r_{H,θ_1,θ_2} is the expression (2.23) of the covariance of an elementary field.

Proof. By definition,

$$\begin{aligned} &C^h_{\alpha,\delta}(\boldsymbol{x})C^h_{\alpha,\delta}(\boldsymbol{y})\mathbb{E}\left[B^h_{\alpha,\delta}(\boldsymbol{x})B^h_{\alpha,\delta}(\boldsymbol{y})\right] \\ &= \int_{\mathbb{R}^2} (\mathrm{e}^{\mathrm{j}\langle \boldsymbol{x},\boldsymbol{\xi}\rangle}-1)\frac{\mathbb{1}_{[\theta_1(\boldsymbol{x}),\theta_2(\boldsymbol{x})]}(\arg\boldsymbol{\xi})}{\|\boldsymbol{\xi}\|^{h(\boldsymbol{x})+1}}(\mathrm{e}^{\mathrm{j}\langle \boldsymbol{y},\boldsymbol{\xi}\rangle}-1)\frac{\mathbb{1}_{[\theta_1(\boldsymbol{y}),\theta_2(\boldsymbol{y})]}(\arg\boldsymbol{\xi})}{\|\boldsymbol{\xi}\|^{h(\boldsymbol{y})+1}}\,\mathrm{d}\boldsymbol{\xi}\,. \end{aligned}$$

Note that, if $\min(\theta_2(\boldsymbol{x}),\theta_2(\boldsymbol{y})) < \max(\theta_1(\boldsymbol{x}),\theta_1(\boldsymbol{y}))$ then

$$\mathbb{1}_{[\theta_1(\boldsymbol{x}),\theta_2(\boldsymbol{x})]}(\arg\boldsymbol{\xi})\mathbb{1}_{[\theta_1(\boldsymbol{y}),\theta_2(\boldsymbol{y})]}(\arg\boldsymbol{\xi}) = 0\,,$$

whereas if $\min(\theta_2(\boldsymbol{x}),\theta_2(\boldsymbol{y}) \geq \max(\theta_1(\boldsymbol{x}),\theta_1(\boldsymbol{y}))$, one has

$$\mathbb{1}_{[\theta_1(\boldsymbol{x}),\theta_2(\boldsymbol{x})]}(\arg\boldsymbol{\xi})\mathbb{1}_{[\theta_1(\boldsymbol{y}),\theta_2(\boldsymbol{y})]}(\arg\boldsymbol{\xi}) = \mathbb{1}_{[\max(\theta_1(\boldsymbol{x}),\theta_1(\boldsymbol{y})),\min(\theta_2(\boldsymbol{x}),\theta_2(\boldsymbol{y}))]}(\arg\boldsymbol{\xi})\,,$$

which directly implies that, in this case,

$$\begin{aligned} &C^h_{\alpha,\delta}(\boldsymbol{x})C^h_{\alpha,\delta}(\boldsymbol{y})\mathbb{E}\left[B^h_{\alpha,\delta}(\boldsymbol{x})B^h_{\alpha,\delta}(\boldsymbol{y})\right] \\ &= \int_{\mathbb{R}^2} (\mathrm{e}^{\mathrm{j}\langle \boldsymbol{x},\boldsymbol{\xi}\rangle}-1)(\mathrm{e}^{\mathrm{j}\langle \boldsymbol{y},\boldsymbol{\xi}\rangle}-1)\frac{\mathbb{1}_{[\max(\theta_1(\boldsymbol{x}),\theta_1(\boldsymbol{y})),\min(\theta_2(\boldsymbol{x}),\theta_2(\boldsymbol{y}))]}(\arg\boldsymbol{\xi})}{\|\boldsymbol{\xi}\|^{h(\boldsymbol{x})+h(\boldsymbol{y})+2}}\,\mathrm{d}\boldsymbol{\xi}\,. \end{aligned}$$

We now use the explicit expression of the covariance of an elementary field given in Proposition 2.15, which reads

$$\begin{aligned} \mathrm{Cov}(Y_{H,\theta_1,\theta_2}(x)Y_{H,\theta_1,\theta_2}(y)) &= \int_{\mathbb{R}^2} (\mathrm{e}^{\mathrm{j}\langle \boldsymbol{x},\boldsymbol{\xi}\rangle}-1)(\mathrm{e}^{\mathrm{j}\langle \boldsymbol{y},\boldsymbol{\xi}\rangle}-1)\mathbb{1}_{[\theta_1,\theta_2]}(\arg\boldsymbol{\xi})\|\boldsymbol{\xi}\|^{-2H-2}\,\mathrm{d}\boldsymbol{\xi} \\ &= r_{H,\theta'_1,\theta'_2}(\boldsymbol{x},\boldsymbol{y})\,. \end{aligned}$$

We then set $H \equiv \frac{h(\boldsymbol{x})+h(\boldsymbol{y})}{2}$, $\theta'_1 \equiv \max(\theta_1(\boldsymbol{x}),\theta_1(\boldsymbol{y}))$ and $\theta'_2 \equiv \min(\theta_2(\boldsymbol{x}),\theta_2(\boldsymbol{y}))$ in the last equality, and by identification we get the result. ∎

Let us explicit the normalized function involving in the definition of the LAFBF (2.7):

$$C^h_{\alpha,\delta}(\boldsymbol{x}) \stackrel{\mathrm{def}}{=} \left(2^{2h(\boldsymbol{x})}\gamma(h(\boldsymbol{x}))C_{h(\boldsymbol{x}),\alpha(\boldsymbol{x})-\delta(\boldsymbol{x}),\alpha(\boldsymbol{x})+\delta(\boldsymbol{x})}(\arg\boldsymbol{x})\right)^{1/2}\,, \tag{2.25}$$

with $\gamma(H)$ defined by (2.22) and C_{H,θ_1,θ_2} defined by (2.21). Then, we have the following corollary:

Corollary 2.16. *The variance of the LAFBF is*

$$\mathrm{Var}\left[B^h_{\alpha,\delta}(\boldsymbol{x})\right] = \frac{2v_{h(\boldsymbol{x}),\alpha(\boldsymbol{x})-\delta(\boldsymbol{x}),\alpha(\boldsymbol{x})+\delta(\boldsymbol{x})}(\boldsymbol{x})}{C^h_{\alpha,\delta}(\boldsymbol{x})^2} = \|\boldsymbol{x}\|^{2h(\boldsymbol{x})}\,, \tag{2.26}$$

where the variogram v is given by (2.20).

3. Wavelet-based orientation of a Gaussian field. Our notion of orientation of a Gaussian field, that we developed in our previous paper [39], is based on a Riesz wavelet analysis and is an extension of the notion proposed in [48]. It is based on the monogenic wavelet analysis. In subsection 3.1 we first present the way we construct isotropic wavelet and give the Riesz wavelet decomposition and its coefficients, then in subsection 3.2 we apply this wavelet decomposition to general self-similar Gaussian field with stationary increments (H-sssi fields) and give the correlation between the random wavelet coefficients of the field, which enables to define a notion of orientation of the latter. Finally, in subsection 3.3 we extend this notion of orientation to every localizable field, by assigning locally the orientation of its tangent fields which are by construction self-similar with stationary increments.

3.1. Wavelets. The starting point of the definition of our notion of wavelet based orientation is the use of isotropic wavelet bases whose existence is proved in [40, 34, 50, 43, 19, 49]. For practical implementation, [48] proposes to define a wavelet tight frame in the following way:

PROPOSITION 3.1. *Let $h(\lambda)$ be a real radial frequency profile such that*

- $\varphi(\lambda) = 0$, $\forall \lambda > \pi$.
- $\sum_{j\in\mathbb{Z}} |\varphi(2^j\lambda)|^2 = 1, \quad \forall \lambda$.
- $\forall n = 0, \cdots, N, \quad \varphi^{(n)}(0) = 0, \forall \lambda$.

Then, the real isotropic wavelet ψ defined by its 2-D Fourier transform $\widehat{\psi}(\boldsymbol{\xi}) = \varphi(\|\boldsymbol{\xi}\|)$, generates a tight wavelet frame of $L^2(\mathbb{R}^2)$ whose basis functions $\psi_{i,\boldsymbol{k}}(\boldsymbol{x}) = 2^i\psi(2^i\boldsymbol{x}-\boldsymbol{k})$ are isotropic with vanishing moments up to order N.

The tight frame property means that any function f belonging to $L^2(\mathbb{R}^2)$ can be expanded as

$$f(\boldsymbol{x}) = \sum_{i,\boldsymbol{k}} \langle f, \psi_{i,\boldsymbol{k}}\rangle \psi_{i,\boldsymbol{k}}(\boldsymbol{x}) \ ,$$

and one has $\|f\|_{L^2} = \sum_{i,\boldsymbol{k}} |c_{i,\boldsymbol{k}}|^2$ where

$$c_{i,\boldsymbol{k}}(f) \stackrel{\text{def}}{=} \langle f, \psi_{i,\boldsymbol{k}}\rangle \ , \tag{3.1}$$

denote the wavelet coefficients of the function f.

The Riesz-based wavelet coefficients of a given function $f \in L^2(\mathbb{R}^2)$ in vector tight wavelet frame $\{\mathcal{R}\psi_{i,\boldsymbol{k}}\}$ are then defined as:

$$c^{(\mathcal{R})}_{i,\boldsymbol{k}}(f) = \begin{pmatrix} c^{(1)}_{i,\boldsymbol{k}}(f) \\ c^{(2)}_{i,\boldsymbol{k}}(f) \end{pmatrix} \ , \tag{3.2}$$

with $c^{(1)}_{i,\boldsymbol{k}}(f) = \langle f, \mathcal{R}_1\psi_{i,\boldsymbol{k}}\rangle$ and $c^{(2)}_{i,\boldsymbol{k}}(f) = \langle f, \mathcal{R}_2\psi_{i,\boldsymbol{k}}\rangle$.

3.2. Orientation of a H-sssi field. We now define our notion of orientation in the case of a Gaussian field admitting stationary increments (H-sssi). It is directly related to the concept of anisotropy, which is encoded in spectral density function f of the random field X with harmonizable representation (1.1).

PROPOSITION 3.2. *Let $H \in (0,1)$ and X a H–self-similar Gaussian field with stationary increments admitting a spectral density f_X. Then f_X is of the form*

$$f_X(\boldsymbol{\xi}) = \|\boldsymbol{\xi}\|^{-2H-2} C_X\left(\frac{\boldsymbol{\xi}}{\|\boldsymbol{\xi}\|}\right) \ ,$$

where C_X is an homogeneous function defined on the sphere $\mathbb{S}^1 = \{\boldsymbol{\xi} \in \mathbb{R}^2, \|\boldsymbol{\xi}\| = 1\}$. The function C_X is called the anisotropy function of X.

Proof. The proof was given in our previous paper [39, Proposition 6]. ∎

Let $\{\psi_{i,\boldsymbol{k}}\}$ be an isotropic tight wavelet frame as defined in subsection 3.1, and $\{\psi^{(\mathcal{R})}_{i,\boldsymbol{k}}\}$ the corresponding vector valued Riesz-based wavelet tight frame generated by $\mathcal{R}\psi$. Our notion of wavelet-based orientation of a self-similar Gaussian field will be based on the following preliminary result, leading to a new formulation for the structure tensor.

THEOREM 3.3. *Let X be a H–self-similar Gaussian field admitting a spectral density f_X. Then, the Riesz-based wavelet coefficients of X, $c_{i,\boldsymbol{k}}^{(\mathcal{R})}(X)$, in the vector wavelet tight frame $\{\psi_{i,\boldsymbol{k}}^{(\mathcal{R})}\}$, are well-defined.*
Moreover, for all $i \in \mathbb{Z}$, the covariance matrix of the $c_{i,\boldsymbol{k}}^{(\mathcal{R})}$ is

$$\boldsymbol{\Sigma}(c_{i,\boldsymbol{k}}^{(\mathcal{R})}(X)) = \mathbb{E}\left(c_{i,\boldsymbol{k}}^{(\mathcal{R})}(f) c_{i,\boldsymbol{k}}^{(\mathcal{R})}(f)^*\right) , \tag{3.3}$$

which reads:

$$\boldsymbol{\Sigma}(c_{i,\boldsymbol{k}}^{(\mathcal{R})}(X)) = 2^{-2i(H+1)} \left[\int_0^{+\infty} \frac{|\varphi(r)|^2}{r^{2H+1}}\,\mathrm{d}r\right] \mathbf{J}(X) ,$$

where for any $\ell_1, \ell_2 \in \{1,2\}$,

$$[\mathbf{J}(X)]_{\ell_1,\ell_2} = \int_{\boldsymbol{\Theta}\in\mathbb{S}^1} \Theta_{\ell_1}\Theta_{\ell_2}\; C_X(\boldsymbol{\Theta})\,\mathrm{d}\boldsymbol{\Theta} , \tag{3.4}$$

with the notation $\boldsymbol{\Theta} = (\Theta_1, \Theta_2)$.
$\mathbf{J}(X)$ is a non-negative definite 2×2 matrix depending only on the anisotropy function C_X and will be called the structure tensor of X.

Proof. The proof was given in our previous paper [39, Theorem 1]. ∎

Observe that our structure tensor does not depend on the chosen isotropic wavelet. It is then an intrinsic characteristic of the Gaussian field X. It will be estimated using the empirical moments of the monogenic wavelet coefficients of the Gaussian field X. We now define the wavelet based orientation of X and its coherency index.

DEFINITION 3.4. *Let $\mathbf{J}(X)$ be the structure tensor of X and λ_1, λ_2 its two eigenvalues. The coherency index of X is*

$$\chi(X) = \frac{|\lambda_2 - \lambda_1|}{\lambda_1 + \lambda_2} .$$

An orientation $\vec{\boldsymbol{n}}$ will be any unit eigenvector associated to the largest eigenvalue of $\mathbf{J}(X)$ or equivalently of $\boldsymbol{\Sigma}(c_{i,\boldsymbol{k}}^{(\mathcal{R})}(X))$.

Example: Orientation of an elementary field
We proved that an elementary field, whose anisotropy function is given by

$$C_X(\boldsymbol{\Theta}) = \frac{1}{4\delta}\left(\mathbb{1}_{[\alpha_0-\delta,\alpha_0+\delta]}(\arg\boldsymbol{\Theta}) + \mathbb{1}_{[\alpha_0+\pi-\delta,\alpha_0+\pi+\delta]}(\arg\boldsymbol{\Theta})\right) ,$$

has for tensor of structure

$$\mathbf{J}(X) = \mathbf{R}_{\alpha_0}\mathrm{diag}\left(\frac{1}{2} + \frac{1}{2}\frac{\sin(2\delta)}{2\delta}, \frac{1}{2} - \frac{1}{2}\frac{\sin(2\delta)}{2\delta}\right)\mathbf{R}_{\alpha_0}^{\mathsf{T}} , \tag{3.5}$$

thus the orientation of the AFBF and its coherency index are well

$$\vec{n} = (\cos\alpha_0, \sin\alpha_0)^{\mathsf{T}}, \quad \chi(X) = \frac{\sin(2\delta)}{2\delta} ,$$

which tends to 1 when the cone width δ tends to zero.

3.3. Local orientation of a localizable random field. We now extend the notion of intrinsic orientation, that we defined for H-sssi fields in a much more general setting, that of localizable Gaussian field. It allows us to define the wavelet-based local orientation of any localizable Gaussian field X at almost any point $\boldsymbol{x_0}$:

DEFINITION 3.5 (Localizable field orientations). *Let X be a Gaussian field with continuous sample paths. Assume that X is localizable at the point $\boldsymbol{x_0}$, with tangent field $Y_{\boldsymbol{x_0}}$, and that $Y_{\boldsymbol{x_0}}$ is a self-similar Gaussian field with stationary increments. One then defines:*

- *The local anisotropy function $S_{\boldsymbol{x_0}}$ at $\boldsymbol{x_0}$ of the localizable Gaussian field X is the anisotropy function of its tangent field $Y_{\boldsymbol{x_0}}$.*
- *The local structure tensor $\mathbf{J}_{\boldsymbol{x_0}}(X)$ at $\boldsymbol{x_0}$ of the localizable Gaussian field X is the structure tensor of its tangent field $Y_{\boldsymbol{x_0}}$.*
- *A local orientation at $\boldsymbol{x_0}$ of the localizable Gaussian field X is any orientation of its tangent field $Y_{\boldsymbol{x_0}}$.*

In view of this definition and of Theorem 2.10, we deduce that any localisable Gaussian field X admits a local orientation at almost every point $\boldsymbol{x_0} \in \mathbb{R}^2$.

Example: Orientations of a LAFBF
The LAFBF has for orientation at point $\boldsymbol{x_0}$ the same orientation than its tangent field at this point, which is an elementary field, so from the previous example we get that $\vec{\boldsymbol{n}}(\boldsymbol{x_0}) = (\cos\alpha(\boldsymbol{x_0}), \sin\alpha(\boldsymbol{x_0}))^{\mathsf{T}}$.

We now illustrate the relevance of our new notion of orientation. To this end, we need to describe some procedure of synthesis which is the purpose of the next section.

4. GAFBF and LAFBF synthesis. To simulate the GAFBF model, the idea is to adopt a *local* strategy, based on the tangent field. This idea was exploited for the simulation of multifractional brownian motion (MBM) in [35]. Indeed, the MBM locally behaves as a fractional brownian motion (FBM); that is formally, the tangent field of a MBM with Hurst function $t \mapsto h(t)$ at point t_0 is a FBM with Hurst index $H_0 = h(t_0)$. Then, to simulate a trajectory of a MBM $B^{h(t)}$ at the discretization points $t_i = \frac{i}{N}$, one can synthesis N FBM B^{H_i} with parameters $H_i = h(t_i)$, from the same Gaussian entries, and assign approximately

$$B^h(t_i) \leftarrow B^{H_i}\left(\frac{i}{N}\right) = B^{h\left(\frac{i}{N}\right)}\left(\frac{i}{N}\right) . \tag{4.1}$$

The N FBM being obtained on a regular grid by Perrin's exact simulation [36] improving [13, 52, 15]. This technique has then been extended to the 2-D case, the multifractional brownian field (MBF) being approached by a fractional brownian field (FBF) which can be obtained as well exactly by Stein's algorithm [46]. These procedures are illustrated in Figure 4. Then, the tangent field formulation reveals not only to be a tool analysis but also a synthesis tool: a localizable field X admitting a tangent field at point $\boldsymbol{x}_0$, that is from (2.12)

$$\left\{\frac{X(\boldsymbol{x_0}+\rho\boldsymbol{x}) - X(\boldsymbol{x_0})}{\rho^H}\right\}_{\boldsymbol{x}\in\mathbb{R}^2} \xrightarrow[\rho\to 0]{d} \left\{Y_{\boldsymbol{x_0}}(\boldsymbol{x})\right\}_{\boldsymbol{x}\in\mathbb{R}^2} ,$$

can be simulated by assigning

$$X(\boldsymbol{x}_0) \leftarrow Y_{\boldsymbol{x}_0}(\boldsymbol{x} = \boldsymbol{x}_0) . \tag{4.2}$$

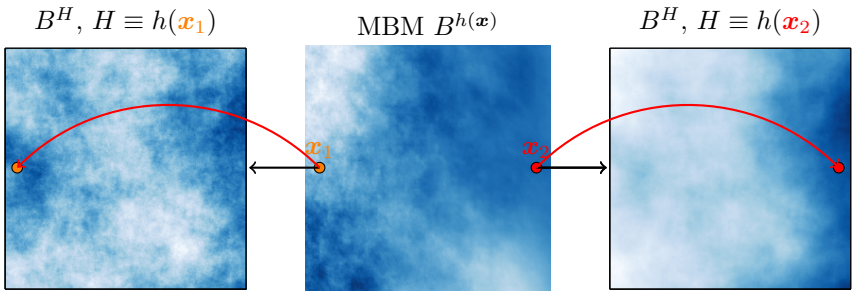

Fig. 4: Simulation of MBF by the tangent field approximation: at each pixel is assigned the corresponding value of its tangent field which is a FBF.

We apply this method to the GAFBF model X and its tangent fields $Y_{\boldsymbol{x}_0}$ whose expressions are given in (2.2) and Proposition 2.11 by:

$$X(\boldsymbol{x}) = \int_{\mathbb{R}^2} (\mathrm{e}^{\mathrm{j}\langle \boldsymbol{x}, \boldsymbol{\xi}\rangle} - 1) \frac{C(\boldsymbol{x}, \boldsymbol{\xi})}{\|\boldsymbol{\xi}\|^{h(\boldsymbol{x})+1}} \widehat{\mathbf{W}}(\mathrm{d}\boldsymbol{\xi}) \,,$$
$$Y_{\boldsymbol{x_0}}(\boldsymbol{x}) = \int_{\mathbb{R}^2} (\mathrm{e}^{\mathrm{j}\langle \boldsymbol{x}, \boldsymbol{\xi}\rangle} - 1) \frac{C(\boldsymbol{x_0}, \boldsymbol{\xi})}{\|\boldsymbol{\xi}\|^{h(\boldsymbol{x_0})+1}} \widehat{\mathbf{W}}(\mathrm{d}\boldsymbol{\xi}) \,.$$

The tangent fields are $h(\boldsymbol{x}_0)$-sssi fields, thus we need a procedure simulation for H-sssi fields we expose in the next section.

4.1. Simulation of H-sssi fields by the turning band method. A recent fast method has been proposed in [7] to simulate AFBF including H-sssi fields, called the turning band method.

Definition 4.1 (Anisotropic Fractional Brownian Fields).
An Anisotropic Fractional Brownian Fields (AFBF) is a Gaussian fields X, with stationary increments and satisfying $X(\mathbf{0}) = 0$ a.s, of the form

$$X(\boldsymbol{x}) = \int_{\mathbb{R}^2} \left(\mathrm{e}^{\mathrm{j}\langle \boldsymbol{x}, \boldsymbol{\xi}\rangle} - 1\right) f(\boldsymbol{\xi})^{1/2} \, \widehat{\mathbf{W}}(\mathrm{d}\boldsymbol{\xi}) \,,$$

where

$$f(\boldsymbol{\xi}) = c(\arg \boldsymbol{\xi}) \, \|\boldsymbol{\xi}\|^{-2h(\arg \boldsymbol{\xi})-2} \,, \tag{4.3}$$

with c and h π-periodic function defined on $(-\pi/2, \pi/2]$ respectively to $\mathbb{R}^+$ and $(0, 1)$.

Remark 4.2. The class of H-sssi fields is included in the AFBF where $h \equiv H$ is constant. Then the following procedure simulation of AFBF holds for H-sssi fields.

The authors of [7] showed that an AFBF can be approximated by a weighted sum of independent Fractional Brownian Fields rotating around the origin. To this

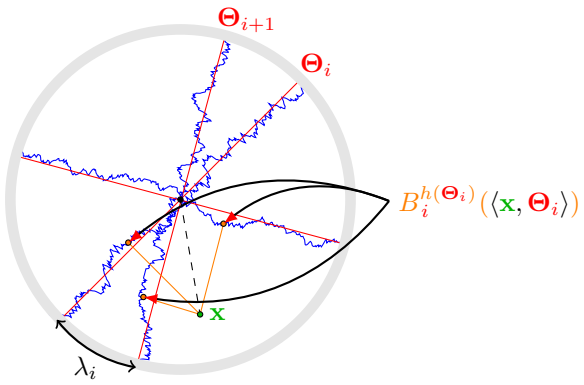

Fig. 5: Turning bands method illustration.

purpose, one can rewrite the semi-variogram in polar coordinates

$$
\begin{aligned}
v_X(\boldsymbol{x}) &= \frac{1}{2}\int_{\mathbb{R}^2} \left|\mathrm{e}^{\mathrm{j}\langle \boldsymbol{x},\, \boldsymbol{\xi}\rangle} - 1\right|^2 f(\boldsymbol{\xi})\,\mathrm{d}\boldsymbol{\xi}\ , \\
&= \frac{1}{2}\int_{-\frac{\pi}{2}}^{\frac{\pi}{2}} \gamma(h(\theta))c(\theta)\left|\langle \boldsymbol{x},\, \boldsymbol{u}(\theta)\rangle\right|^{2h(\theta)}\mathrm{d}\theta\ , \\
&= \int_{-\frac{\pi}{2}}^{\frac{\pi}{2}} \widetilde{v}_\theta(\langle \boldsymbol{x},\, \boldsymbol{u}(\theta)\rangle)\,\mathrm{d}\theta\ ,
\end{aligned}
\tag{4.4}
$$

where we denote $\widetilde{v}_\theta(t) = \gamma(h(\theta))c(\theta)|t|^{2h(\theta)}$, $\boldsymbol{u}(\theta) = (\cos\theta, \sin\theta)^\mathsf{T}$ and $\gamma(H)$ defined by (2.22). Ignoring the factor $\gamma(h(\theta))c(\theta)$, one can recognize that $\tilde{v}_\theta$ is the variogram of a FBM of order $h(\theta)$, which is rotating around the origin $\theta = -\pi/2, \ldots, \pi/2$. Then, it is natural to consider the following Gaussian field:

$$
X_{\Theta,\Lambda}(\boldsymbol{x}) = \sum_{i=1}^{n} \sqrt{\lambda_i \gamma(h(\Theta_i))c(\Theta_i)} B_i^{h(\Theta_i)}\left(\langle \boldsymbol{x},\, \boldsymbol{u}(\Theta_i)\rangle\right)\ ,
\tag{4.5}
$$

where the n radial bands $\Theta = (\Theta_i)_{1\leqslant i\leqslant n}$ are a discrete angles sampling on which is projected the point $\boldsymbol{x}$ (see Figure 5), $\lambda_i = \Theta_{i+1} - \Theta_i$ are the band widths, and the $B_i^{h(\theta_i)}$ are n independent FBM of order $h(\Theta_i)$; whose variogram is:

$$
v_{\Theta,\Lambda}(\boldsymbol{x}) = \sum_{i=1}^{n} \lambda_i \gamma(h(\Theta_i))c(\Theta_i) v_{h(\Theta_i)}\left(\langle \boldsymbol{x},\, \boldsymbol{u}(\Theta_i)\rangle\right)\ ,
$$

which can be viewed in turn as approximation by the rectangle method of the integral (4.4). This discrete version is a good approximation, provided $\max_i(\Theta_{i+1} - \Theta_i) \leqslant \varepsilon$ for ε sufficiently small. Theoretical guarantees based on the Kolmogorov distance are detailed in [7]. This result shall be crucial when simulating this Gaussian model.:

$$
X_{\Theta,\Lambda}(\boldsymbol{x}) = \sum_{i=1}^{n} \omega_i B_i^{h(\Theta_i)}\left(\langle \boldsymbol{x},\, \boldsymbol{u}(\Theta_i)\rangle\right)\ ,
\tag{4.6}
$$

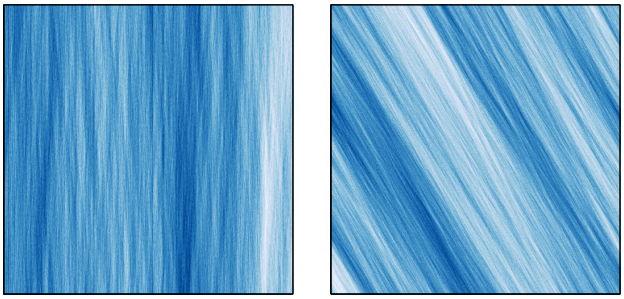

Fig. 6: Simulation of an elementary field with turning band method for Hurst index $H = 0.2$, accuracy $\delta = 10^{-1}$, approximation error $\epsilon = 3.10^{-2}$, direction $\alpha_0 = 0$ (on the left) and $\alpha_0 = \frac{\pi}{6}$ (on the right)

where $\omega_i = \sqrt{\lambda_i \gamma(h(\Theta_i))c(\Theta_i)}$ contribute to a weighted sum of the n $B_i^{h(\Theta_i)}$ independent FBM bands as illustrated in Figure 5.

Simulation. Let us simulate $X_{\Theta,\Lambda}$ on $[0,1]^2$ sampling on a grid $r^{-1}\mathbb{Z}^2 \cap [0,1]^2$ of size $r \times r$ with $r = 2^k - 1, k \in \mathbb{N}^\star$, whose points are $\boldsymbol{x} = (k_1/r, k_2/r)^\mathsf{T}$ with $0 \leqslant k_1, k_2 \leqslant r$. The FBM $B_i^{h(\theta_i)}$ synthesis also requires to simulate these process on a regular grid, which is not satisfied by the argument $\langle \boldsymbol{x}, \boldsymbol{u}(\Theta_i) \rangle$ in (4.6). To overcome this problem, the trick is to choose Θ_i such that $\tan(\Theta_i) = p_i/q_i$ where $p_i \in \mathbb{Z}$ and $q_i \in \mathbb{N}$. Then, by self-similarity of the $B_i^{h(\theta_i)}$, they obtain:

$$\begin{aligned} &\left\{ B_i^{h(\theta_i)} \left(\frac{k_1}{r} \cos\Theta_i + \frac{k_2}{r} \sin\Theta_i \right) ;\ 0 \leqslant k_1, k_2 \leqslant r \right\} \\ &\stackrel{\mathcal{L}}{=} \left(\frac{\cos\Theta_i}{r q_i} \right)^{h(\theta_i)} \left\{ B_i^{h(\theta_i)} \left(k_1 q_i + k_2 p_i \right) ;\ 0 \leqslant k_1, k_2 \leqslant r \right\} , \end{aligned}$$

where $k_1 q_i + k_2 p_i$ are now integers. So it reduces to a regular sampling of $B_i^{h(\theta_i)}(k)$ for integers $0 \leqslant k \leqslant r(|p_i| + q_i)$, which can be performed by a circulant matrices method using the fast algorithm of Perrin *et al.* [36] on a regular grid.

Complexity. The choice of the bands orientations $(\Theta_i)_{1 \leqslant i \leqslant n}$ is governed by the global computational cost of the B_i^H, within dynamic programming [7]. The turning band method is used here to simulate the textures of Figure 6 which are elementary fields $Y_{H,\alpha_0-\delta,\alpha_0+\delta}$ with global orientation $\alpha_0 = 0$ and $\alpha_0 = \frac{\pi}{6}$, for δ constant (for effects from tuning δ see Figure 2). Once the n Fractional Brownian Field B_i^H of length ℓ_i are generated, with a complexity in $n\ell \log \ell$ where $\ell = \max_i \ell_i$, then the algorithm for simulating $Y^{[n]}_{H,\theta_1,\theta_2}$ is very fast since it requires only $\mathrm{Card}\{i : \omega_i^{\theta_1,\theta_2} \neq 0\} \times r^2 = O(r^2)$ operations with r^2 the number of pixels of the image.

4.2. Simulation of the GAFBF. The tangent field of the GAFBF X (2.2) at a point $\boldsymbol{x}_0$ is a H-sssi field $Y_{\boldsymbol{x}_0}$ (2.15), which can be simulated by the turning band method described in subsection 4.1, with anisotropy function $C(\boldsymbol{x_0}, \cdot)$ and constant

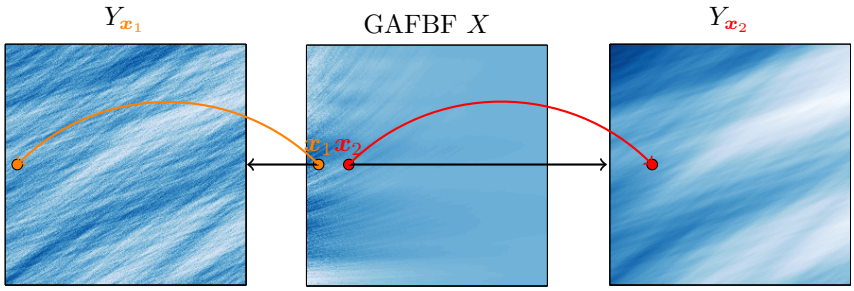

Fig. 7: GAFBF simulation: for each pixel, we assign the corresponding value of its tangent field. Here is an example with $\alpha(x_1, x_2) = -\frac{\pi}{2} + x_1$, $h(x_1, x_2) = 0.1 + 0.5x_1$, $\delta = 10^{-1}$.

Hurst index $h(\boldsymbol{x}_0)$:

$$Y_{\boldsymbol{x}_0}(\boldsymbol{x}) = \int_{\mathbb{R}^2} (\mathrm{e}^{\mathrm{j}\langle \boldsymbol{x},\, \boldsymbol{\xi}\rangle} - 1) \frac{C(\boldsymbol{x_0}, \boldsymbol{\xi})}{\|\boldsymbol{\xi}\|^{h(\boldsymbol{x_0})+1}} \widehat{\mathbf{W}}(\mathrm{d}\boldsymbol{\xi}) \tag{4.7}$$

$$\approx \sum_{i=1}^{n} \sqrt{\lambda_i \gamma(h(\boldsymbol{x_0})) C(\boldsymbol{x_0}, \Theta_i)} B_i^{h(\boldsymbol{x_0})} \left(\langle \boldsymbol{x},\, \boldsymbol{u}(\Theta_i) \rangle \right) \equiv Y_{\boldsymbol{x}_0}^{[n]}(\boldsymbol{x}) \ . \tag{4.8}$$

Then, for each point of the grid, we assign the corresponding value of its tangent field at this point:

$$X(\boldsymbol{x}_0) \leftarrow Y_{\boldsymbol{x}_0}(\boldsymbol{x} = \boldsymbol{x}_0) \approx Y_{\boldsymbol{x}_0}^{[n]}(\boldsymbol{x}_0) \ . \tag{4.9}$$

All these fields has to be generated from the same Gaussian entries. The algorithm is described in ... We need to generate as much FBM there are pixels, which is costly. Its complexity is ... An example is depicted in Figure 7.

4.3. Simulation of the LAFBF. The LAFBF is a particular case of GAFBF where the anisotropy function is a cone. We will see in this section that the LAFBF synthesis can be realized either by the Cholesky method in subsection 4.3.1 to the extent that we have the expression of the covariance in Proposition 2.15, either by using a suitable coupling of the tangent field and the turning bands approximations with a krigeage taking into account the spatial covariance structure. We focus on the latter in subsection 4.3.2, since it provides a way to simulate the LAFBF with a better complexity than the Cholesky one which has a high computational cost and improve the general procedure provide in subsection 4.2. A similar strategy have been used by [11] to simulate the MBM. The idea is to avoid having to simulate of all the tangents fields in each of the points, but only in a few points and then to make an interpolation for the others. More precisely, in (4.1) we do not generate all the n FBM with order $H_i = h(i/N)$, but only $U < n$ FBM with order respectively $H_1, \ldots, H_U$, for example evenly distributed $H_u = u/(U+1)$. Then, at each location $t_i = i/N$ we specify a set of neighbors $\mathcal{V}_i = \{(v,k)\}$ and can predict the value by interpolation:

$$B^h(t_i) = \sum_{(v,k)\in\mathcal{V}_i} \gamma_{v,k}^{(i)} B^{H_v}(t_k) \ ,$$

whose weights are obtained by a mean squared error criterion using the knowledge of the covariance structure. As well, from the tangent field synthesis method (4.9), since we know the covariance of the LAFBF, we are able to avoid the simulation of as many tangent fields as there are pixels by the following procedure:

1. Simulate U LAFBF with orientation function α, directionality function δ and *constant* Hurst function H_u, each of them obtained as for (4.9) by assigning

$$B^{H_u}_{\alpha,\delta}(\boldsymbol{x_0}) \leftarrow Y^{[n]}_{H_u,\alpha(\boldsymbol{x_0})-\delta(\boldsymbol{x_0}),\alpha(\boldsymbol{x_0})+\delta(\boldsymbol{x_0})}(\boldsymbol{x}=\boldsymbol{x_0})\ , \tag{4.10}$$

   where the tangent fields are elementary fields (2.16) at each pixel. We will show that these fields $B^{H_u}_{\alpha,\delta}$ can be simulated as much efficiently as a single H-sssi field (by the turning bands method seen in subsection 4.1), due to the fact that H_u remains constant for all the pixels of the elementary fields.

2. We finally simulate $B^h_{\alpha,\delta}$ where h may varies, by a kriging method which exploit the covariance to interpolate the samples $(B^{H_u}_{\alpha,\delta})_{1\leqslant u\leqslant U}$.

We will detail separately these two steps in subsection 4.3.2 and subsection 4.3.3.

4.3.1. Cholesky method. We gave in Proposition 2.13, Proposition 2.14 and Proposition 2.15 explicit formulas for both the covariance of the elementary fields and the LAFBF. Therefore, applying the classical Cholesky method (see Appendix A) enables the simulation of oriented texture with size 127×127, as illustrated in Figure 8 where H and δ are constants and α is a given orientation function. For the elementary fields in Figure 8a and Figure 8b, we recover with the Cholesky method the same kind of textures which have been obtained by the turning band method in Figure 6. For an orientation function $\boldsymbol{x}\in\mathbb{R}^2\mapsto\alpha(\boldsymbol{x})$ which does not vary too fast, such as the one used in Figure 8d, the resulting texture have a good quality and we get the expected local orientations. However, when the variations of the orientation function α are steeper, such as the one used in Figure 8d, the result is no longer completely satisfying in so far as some bands of artifact appear. The reason is the following: for two point $\boldsymbol{x}$ and $\boldsymbol{y}$ in $\mathbb{R}^2$, the random variables $B^h_{\alpha,\delta}(\boldsymbol{x})$ and $B^h_{\alpha,\delta}(\boldsymbol{x})$ are independent as soon as the angle $\alpha(\boldsymbol{x})$ and $\alpha(\boldsymbol{y})$ are far from 2δ (the corresponding cones have disjointed supports), then the covariance matrix $\boldsymbol{\Sigma}=\mathbf{L}\mathbf{L}^\intercal$ is largely sparse and so $\mathbf{L}$ too. Let now $\boldsymbol{Z}$ be a random Gaussian vector, the product $\mathbf{L}\boldsymbol{Z}$ involves different entries of the latter, in a non continuously manner, which creates these bands of grayscale jumps. The Cholesky method has a high computational cost, since it requires to fill a matrix $\mathbf{R}$ of square size $N=r^2$ by calling a covariance function for all entries, and then to execute a Cholesky decomposition matrix whose complexity is in $O(N^3)$.

Remark 4.3. Another way is to use approximated methods based on the covariance matrix, as developed in [10], to speed up the synthesis obtained by the Cholesky method. Unfortunately, these approximations lead to bad results with poor visibles orientations in some regions.

4.3.2. Simulation of a LAFBF with constant Hurst index H. The simulation of a LAFBF with constant Hurst index H following (4.10) requires to compute $Y^{[n]}_{H,\alpha(\boldsymbol{x_0})-\delta(\boldsymbol{x_0}),\alpha(\boldsymbol{x_0})+\delta(\boldsymbol{x_0})}(\boldsymbol{x}=\boldsymbol{x_0})$ at each point $\boldsymbol{x}_0=(k_1/r,k_2/r)^\intercal$, where Y is the tangent field of the LAFBF at this point (2.16), which is a H-sssi elementary field

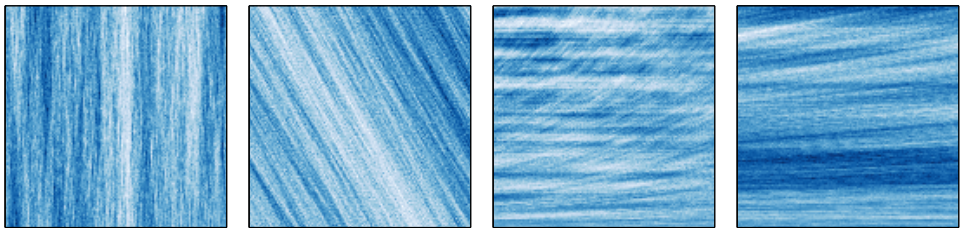

(a) $\alpha_0 = 0$ (b) $\alpha_0 = \frac{\pi}{6}$ (c) $\alpha(\boldsymbol{x}) = -\frac{\pi}{2} + x_2$ (d) $\alpha(\boldsymbol{x}) = -\frac{\pi}{2} + 0.2 \times x_2$

Fig. 8: Simulation of a LAFBF with Cholesky method for constant Hurst index $H = 0.2$, constant accuracy $\delta = 2.10^{-2}$, and different orientation functions.

simulated by (4.5) as:

$$Y^{[n]}_{H,\alpha(\boldsymbol{x_0})-\delta(\boldsymbol{x_0}),\alpha(\boldsymbol{x_0})+\delta(\boldsymbol{x_0})}(\boldsymbol{x} = \boldsymbol{x_0}) = \sum_{i=1}^{n} \sqrt{(\Theta_{i+1} - \Theta_i)\gamma(H)c_{\alpha,\delta}(\boldsymbol{x_0}, \Theta_i)} \left(\frac{\cos\Theta_i}{rq_i}\right)^H B_i^H \left(k_1 q_i + k_2 p_i\right) ,$$

with $c_{\alpha,\delta}$ defined in (2.8) and (2.9), Θ_i the turning bands and B_i^H n independant FBM with order H, computed only once. The advantage to have a constant Hurst index H is that we can always use the same n FBM to compute the contributions for all points $\boldsymbol{x}_0$. Then, in the algorithm subsection 4.3.2, the preprocessing step (instructions 1,2,3,4 in the pseudocode) does not depend on the expected local orientations, includes the dynamic choice and sorting of discrete bands, and the simulation of the n FBM. These steps are executed once and for all. The rest of the algorithm is of complexity $O(r^2 \log n)$. Indeed, at each point (k_1, k_2), a turning band Θ_i contributes to $B^H_{\alpha,\delta}(k_1, k_2)$ if and only if $c_{\alpha,\delta}((k_1, k_2), \Theta_i) \neq 0$, *i.e* $|\Theta_i - \alpha(k_1, k_2)| \leqslant \alpha$. Thus, since the array Θ_i is sorted, one such index i is founded using a binary search, and then the others in its neighborhood. The anisotropy function $c_{\alpha,\delta}(\boldsymbol{x_0}, \Theta_i)$ then play the role of bands selector in each point $\boldsymbol{x}_0$, as illustrated in Figure 9. In order to have a sufficient number of bands in each cone $c_{\alpha,\delta}(\boldsymbol{x_0}, \theta)$, we need the number of bands n around $[-\pi/2, \pi/2]$ to be sufficiently large for having good approximations. Since this step is made once for all, it is recommended to choose a small accuracy parameter ϵ, from which will be generated a large number of bands.

Remark 4.4. We actually needed to consider for $c_{\alpha,\delta}(\boldsymbol{x_0}, \cdot)$ a regularized version of the characteristic function, typically a Gaussian as in Figure 3, to avoid numerical artifacts due to the rectangle method approximation (4.6). Indeed for two orientations sufficiently spaced, the sum (4.6) involves different bands (Θ_i) which creates some grayscale jumps. However for greater Hurst values, we can't get rid of these artifacts as we can see in Figure 10.

4.3.3. Varying Hurst index by kriging method. We now allow $h(x)$ to vary w.r.t. x. In this section, we will briefly describe the kriging method [29, 30, 31, 25]. It was the first spatial interpolation which took into account the spatial dependence of the data, and so is well-suited to simulate the LAFBF. The interpolated value of a random field $Z(\cdot)$ at the unsampled location $\boldsymbol{s_0}$ is calculated from a linear combination

Algorithm 4.1 Simulation of the LAFBF

Input: $r = 2^k - 1$, H, α_0, α, ϵ
Output: $B^H_{\alpha,\delta}$ LAFBF of size $(r+1) \times (r+1)$

```
(p_i, q_i)_{1⩽i⩽n} ← DynamicBandsChoice(r, ε)
Compute and sort angles (Θ_i)_{1⩽i⩽n} : Θ_i ← atan2(p_i, q_i)
Compute width bands (λ_i)_{1⩽i⩽n} : λ_i ← Θ_{i+1} − Θ_i
Generate n FBM : B_i^H ← circFBM(r(|p_i| + |q_i|), H)
Initialization : X ← 0
for all (k_1, k_2) do
    for i = 1 to n do
        ω_i ← sqrt((Θ_{i+1} − Θ_i) γ(H) c_{α,δ}((k_1, k_2), Θ_i)) (cos Θ_i / (r q_i))^H
        B^H_{α,δ}(k_1, k_2) ← B^H_{α,δ}(k_1, k_2) + ω_i B_i^H(k_1 q_i + k_2 p_i)
    end for
end for
```

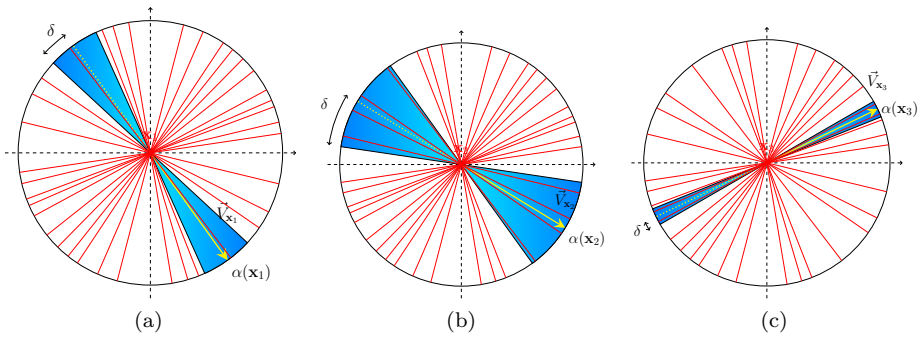

Fig. 9: Graphic illustrating in each point $\boldsymbol{x}_1, \boldsymbol{x}_2, \boldsymbol{x}_3, \ldots$ the bands selection by the local anisotropy function $c_{\alpha,\delta}$ among the n pre-computed red bands.

of the observed values $Z_i = Z(\boldsymbol{s_i})$ in a neighborhood $\mathcal{V}(\boldsymbol{s}_0)$, that is

$$\widehat{Z}(\boldsymbol{s_0}) = \sum_{i \in \mathcal{V}(\boldsymbol{s_0})} \lambda_i Z(s_i) = \boldsymbol{\lambda}^\mathsf{T} \boldsymbol{Z} \ .$$

We assume to know the variance-covariance matrix $\boldsymbol{\Sigma}$ of $\boldsymbol{Z}$ on the neighborhood $\mathcal{V}(\boldsymbol{s_0})$, given by $\boldsymbol{\Sigma}_{ij} = \mathrm{Cov}(Z(\boldsymbol{s_i}), Z(\boldsymbol{s_j}))$ for $\boldsymbol{s_i}, \boldsymbol{s_j} \in \mathcal{V}(\boldsymbol{s_0})$, and the vector $\boldsymbol{c_0} = \mathrm{Cov}[\mathbf{Z}, Z(\boldsymbol{s_0}) \cdot (1, \ldots, 1)^\mathsf{T}]$. The aim is to find weights λ_i for which we have the best linear estimation, whose results hold in the following proposition:

PROPOSITION 4.5. *The estimator $\widehat{Z}(\boldsymbol{s_0})$ is called the BLUE (Best Linear Unbiased Estimator) of $Z(\boldsymbol{s_0})$ if $\boldsymbol{\lambda} = \boldsymbol{\Sigma}^{-1}\boldsymbol{c_0}$, that is*

$$\widehat{Z}(\boldsymbol{s_0}) = \boldsymbol{c_0}^\mathsf{T} \boldsymbol{\Sigma}^{-1} \boldsymbol{Z} \ , \tag{4.11}$$

which verify these properties:

- *The predicted error is non biased*

$$\mathbb{E}\left[\widehat{Z}(\boldsymbol{s_0}) - Z(\boldsymbol{s_0})\right] = 0 \ ,$$

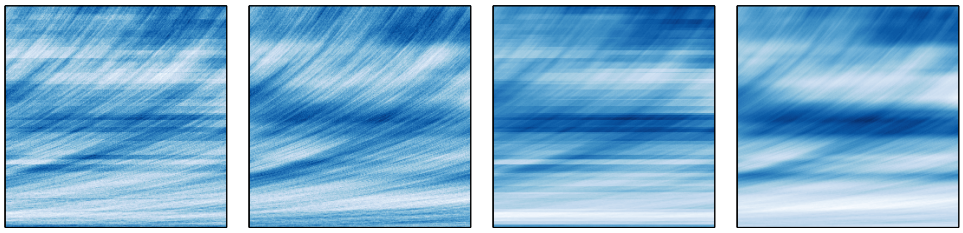

(a) $H = 0.2$ (b) $H = 0.2$ regularized (c) $H = 0.5$ (d) $H = 0.2$ regularized

Fig. 10: Simulation of a LAFBF with tangent field formulation combining the turning band method, for Hurst index constant $H = 0.2$ (top) and $H = 0.5$ (bottom), with (right) or without (left) a regularized Gaussian window, and the orientation function $\alpha_0(x, y) = -\frac{\pi}{2} + y$

- *The predicted error has a minimal variance*

$$\mathrm{Var}\left[\widehat{Z}(\boldsymbol{s_0}) - Z(\boldsymbol{s_0})\right] = \min_{\lambda_i}\left(\mathrm{Var}\left[\sum_{i\in\mathcal{V}(\boldsymbol{s_0})}\lambda_i Z(\boldsymbol{s_i}) - Z(\boldsymbol{s_0})\right]\right) .$$

Proof. See in Appendix B. ∎

Let us now consider the kriging of the LAFBF $B^{h(x,y)}_{\alpha(x,y),\delta(x,y)}(x, y)$ defined for $(x, y) \in [0, 1]^2$ with Hurst function h, orientation function α and a constant accuracy δ. We sample the field on a grid $r^{-1}\mathbb{Z}^2 \cap [0, 1]^2$ with $r = 2^k - 1$, and we generate on this grid, U LAFBF with Hurst index constant $H_u, u = 1, ..., U$: $B^{H_u}_{\alpha(k_1,k_2),\delta(k_1,k_2)}(k_1, k_2)$ for all pixel $(k_1, k_2) \in \{0, ..., r\}^2$.

To obtain an estimation of $B^{h(k_1,k_2)}_{\alpha(k_1,k_2),\delta(k_1,k_2)}(k_1, k_2)$, we first look for the upper and lower bounds of $h(k_1, k_2) : H_u \leqslant h(k_1, k_2) < H_{u+1}$, then we do the kriging of the random field $Z(x, y, z) = B^{h(z)}_{\alpha(x,y),\delta(x,y)}(x, y)$ at the unsample point $\boldsymbol{s_0} = (k_1, k_2, h(k_1, k_2))$ by considering the following neighborhood:

$$\mathcal{V}(\boldsymbol{s_0}) = \left\{ \begin{array}{ccccc} (k_1-1,k_2-1,H_u) & ; & (k_1-1,k_2,H_u) & ; & (k_1-1,k_2+1,H_u) \\ (k_1,k_2-1,H_u) & ; & (k_1,k_2,H_u) & ; & (k_1,k_2+1,H_u) \\ (k_1+1,k_2-1,H_u) & ; & (k_1+1,k_2,H_u) & ; & (k_1+1,k_2+1,H_u) \\ (k_1-1,k_2-1,H_{u+1}) & ; & (k_1-1,k_2,H_{u+1}) & ; & (k_1-1,k_2+1,H_{u+1}) \\ (k_1,k_2-1,H_{u+1}) & ; & (k_1,k_2,H_{u+1}) & ; & (k_1,k_2+1,H_{u+1}) \\ (k_1+1,k_2-1,H_{u+1}) & ; & (k_1+1,k_2,H_{u+1}) & ; & (k_1+1,k_2+1,H_{u+1}) \end{array} \right\}$$

Let fixed $\boldsymbol{s_i} = (x_i, y_i, H_i)$ and $\boldsymbol{s_j} = (x_j, y_j, H_j)$ in $\mathcal{V}(\boldsymbol{s_0})$, then the 18×18 covariance matrix is

$$\begin{aligned} \boldsymbol{\Sigma}_{ij} = \mathrm{Cov}(Z(\boldsymbol{s_i}), Z(\boldsymbol{s_j})) &= \mathrm{Cov}\left(B^{H_i}_{\alpha(x_i,y_i),\delta(x_i,y_i)}, B^{H_j}_{\alpha(x_j,y_j),\delta(x_j,y_j)}\right) , \\ &= r_{H^{ij},\theta_1^{ij},\theta_2^{ij}}((x_i, y_i), (x_j, y_j)) , \end{aligned}$$

where $r_{H^{ij},\theta_1^{ij},\theta_2^{ij}}$ is the covariance of an elementary field with parameters:

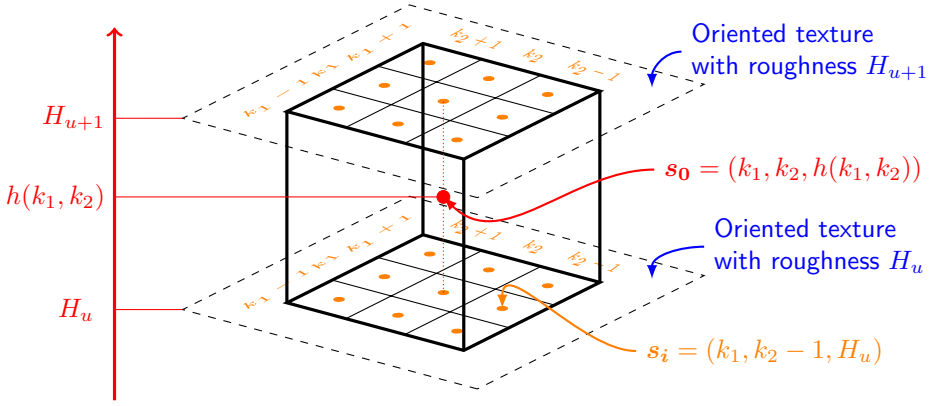

Fig. 11: Representation of the neighborhood $\mathcal{V}(\boldsymbol{s_0})$

$$
\begin{aligned}
H^{ij} &= \frac{h(z_i) + h(z_j)}{2} \ , \\
\theta_1^{ij} &= \max(\alpha(x_i, y_i) - \delta(x_i, y_i), \alpha(x_j, y_j) - \delta(x_j, y_j)) \ , \\
\theta_2^{ij} &= \max(\alpha(x_i, y_i) + \delta(x_i, y_i), \alpha(x_j, y_j) + \delta(x_j, y_j)) \ ,
\end{aligned}
$$

and $\boldsymbol{c_0}$ is the vector of size 1×18 whose components are $\mathrm{Cov}(Z(\boldsymbol{s_i}), Z(\boldsymbol{s_0}))$.

The prediction $\widehat{Z}(\boldsymbol{s_0})$ is given by

$$\widehat{Z}(\boldsymbol{s_0}) = \boldsymbol{c_0}^{\mathsf{T}} \boldsymbol{\Sigma}^{-1} \boldsymbol{Z} \ ,$$

with $\boldsymbol{Z}$ the vector containing the 18 neighbors $Z(\boldsymbol{s_i})$ of $Z(\boldsymbol{s_0})$.
We finally know the variance of the prediction error:

$$
\begin{aligned}
\mathrm{Var}\left[\widehat{Z}(\boldsymbol{s_0}) - Z(\boldsymbol{s_0})\right] &= \left(\boldsymbol{c_0}^{\mathsf{T}} \boldsymbol{\Sigma}^{-1}\right) \boldsymbol{\Sigma} \left(\boldsymbol{\Sigma}^{-1} \boldsymbol{c_0}\right) + \sigma^2 - 2 \boldsymbol{c_0}^{\mathsf{T}} \boldsymbol{\Sigma}^{-1} \boldsymbol{c_0} \ , \\
&= \sigma^2 - \boldsymbol{c_0}^{\mathsf{T}} \boldsymbol{\Sigma}^{-1} \boldsymbol{c_0} \ .
\end{aligned}
$$

Simulation. The algorithm computes the estimation $\widehat{Z}(\boldsymbol{s}_0)$ for each pixel $\boldsymbol{s_0}$ of the image, the results are displayed in Figure 12 for a given orientation function $\boldsymbol{x} \mapsto \alpha(\boldsymbol{x})$ and three different Hurst functions $\boldsymbol{x} \mapsto h(\boldsymbol{x})$ with δ constant or not. This procedure is quite costly because for each pixel $\boldsymbol{s_0}$ it requires to form the covariance matrix $\boldsymbol{\Sigma}$ of size 18×18 (which implies as much calls of the covariance function r_{H,θ_1,θ_2}), and to inverse this matrix. It could be improved by exploiting the GPU's parallel computing architecture, since we have the same procedure for each pixel and we can avoid to compute several times the covariance between adjacent pixels.

5. Another anisotropic model : deformation of a H-sssi field. As we have seen, LAFBF are possibly corrupted by some numerical artifacts, which can compromise the estimation of the orientations. Another way to obtain a random field locally oriented consists in deforming a globally oriented one such as H-sssi fields. This other kind of model that we introduced in [39] is based on the approach developed in Perrin's works [33].

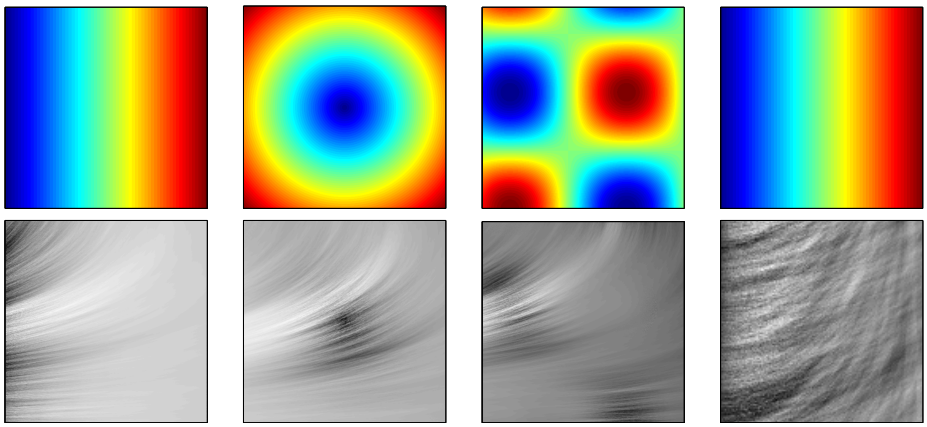

Fig. 12: Simulation of a LAFBF of orientation function $\alpha(x_1, x_2) = -\frac{\pi}{2} + x_1$ with different Hurst functions, and δ constant except for the last one where δ linearly varying.

DEFINITION 5.1 (Warped Anisotropic Fractional Brownian Field). *Let X be a H-sssi field X with anisotropy function C_X and let $\boldsymbol{\Phi}$ be a continuously differentiable function defined from $\mathbb{R}^2$ to $\mathbb{R}^2$. The Warped Anisotropic Fractional Brownian Field (WAFBF) is defined as the deformation of X by $\boldsymbol{\Phi}$:*

$$Z_{\boldsymbol{\Phi},X}(\boldsymbol{x}) = X(\boldsymbol{\Phi}(\boldsymbol{x})), \quad \forall \boldsymbol{x} \in \mathbb{R}^2 \,. \tag{5.1}$$

Simulation. Let us choose for X a standard elementary field with anisotropy function

$$C_X(\boldsymbol{\Theta}) = \frac{1}{4\delta}\left(\mathbb{1}_{[\delta,\delta]}(\arg\boldsymbol{\Theta}) + \mathbb{1}_{[\pi-\delta,\pi+\delta]}(\arg\boldsymbol{\Theta})\right) \,, \tag{5.2}$$

and for the deformation function $\boldsymbol{\Phi}$ a local rotation whose expression is:

$$\boldsymbol{\Phi}(\boldsymbol{x}) = \mathbf{R}_{-\alpha(\boldsymbol{x})}\boldsymbol{x} = \begin{pmatrix} \cos\alpha(\boldsymbol{x})\, x_1 + \sin\alpha(\boldsymbol{x})\, x_2 \\ -\sin\alpha(\boldsymbol{x})\, x_1 + \cos\alpha(\boldsymbol{x})\, x_2 \end{pmatrix} \equiv \begin{pmatrix} \boldsymbol{\Phi}_1(\boldsymbol{x}) \\ \boldsymbol{\Phi}_2(\boldsymbol{x}) \end{pmatrix} \,, \tag{5.3}$$

with $\alpha : \mathbb{R}^2 \to \mathbb{R}$ a C^1 function defined on $\mathbb{R}^2$ such that, on an open set $U \subset \mathbb{R}^2$, we have:

$$\forall \boldsymbol{x_0} \in U, \qquad \nabla\alpha(\boldsymbol{x_0}) \wedge \boldsymbol{x_0} = \frac{\partial\alpha}{\partial x_1}(\boldsymbol{x_0})x_{0,2} - \frac{\partial\alpha}{\partial x_2}(\boldsymbol{x_0})x_{0,1} \neq -1 \,, \tag{5.4}$$

in order to have a non-zero determinant for the jacobian of $\boldsymbol{\Phi}$.

The elementary field X is simulated by the turning band method (see subsection 4.1) and the deformed image is then obtained by:

$$Z_{\boldsymbol{\Phi},X}(\boldsymbol{x}) \approx X_{\Theta,\Lambda}(\boldsymbol{\Phi}(\boldsymbol{x})) = \sum_{i=1}^{n} \sqrt{\lambda_i \gamma(H) c(\Theta_i)} B_i^H(\langle \boldsymbol{\Phi}(\boldsymbol{x}),\, \boldsymbol{u}(\Theta_i)\rangle) \,. \tag{5.5}$$

Thus, the complexity is the same as for a simple elementary field and the simulation of the WAFBF is really efficient. We give some illustrations of textures produce by this procedure in Figure 13. We do not observe artifacts anymore, but the control of

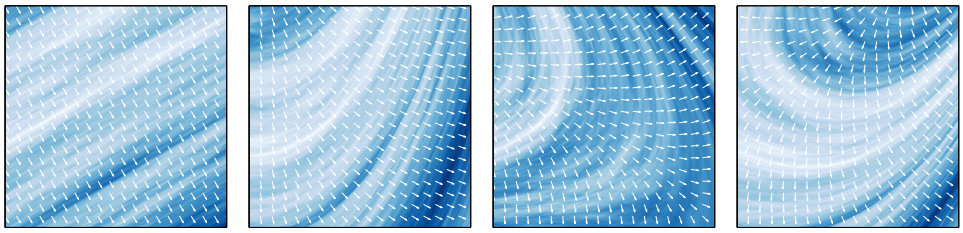

(a) $\alpha(\boldsymbol{x}) = -\frac{\pi}{3}$ (b) $\alpha(\boldsymbol{x}) = -\frac{\pi}{2} + x_1$ (c) $\alpha(\boldsymbol{x}) = -\frac{\pi}{2} + x_2$ (d) $\alpha(\boldsymbol{x}) = -\frac{\pi}{2} + x_1^2 - x_2$

Fig. 13: Simulation of the field $Z(\boldsymbol{x}) = X(\mathbf{R}_{-\alpha(\boldsymbol{x})} \cdot \boldsymbol{x})$, where X is the standart AFBF with $\alpha_0 = 0$, and with the different differentiable functions α.

the anisotropy is no longer insure, so we need to characterize the local orientations.

Local orientation characterization. Let us expose the local anisotropic properties of such Gaussian fields we developed in [39].

PROPOSITION 5.2. *The Gaussian field $Z_{\mathbf{\Phi},X}$ defined by (5.1) is localizable at any point $\boldsymbol{x_0} \in \mathbb{R}^2$, with tangent field $Y_{\boldsymbol{x_0}}$ whose expression is:*

$$Y_{\boldsymbol{x_0}}(\boldsymbol{x}) = X(\mathbf{D\Phi}(\boldsymbol{x_0})\,\boldsymbol{x}), \quad \forall \boldsymbol{x} \in \mathbb{R}^2 \,,$$

where $\mathbf{D\Phi}(\boldsymbol{x_0})$ is the jacobian matrix of $\mathbf{\Phi}$ at point $\boldsymbol{x_0}$.

PROPOSITION 5.3. *Let $Z_{\mathbf{\Phi},X}$ be a WAFBF defined by (5.1) from X an elementary field whose orientation is $\vec{\boldsymbol{n}}$. We assume that the deformation function $\mathbf{\Phi}$ is a C^1-diffeomorphism on an open set $U \subset \mathbb{R}^2$. Then, in each point $\boldsymbol{x}_0 \in U$, an approximation (up to δ) of the local orientation is*

$$\vec{\boldsymbol{n}}_Z(\boldsymbol{x_0}) = \frac{\mathbf{D\Phi}(\boldsymbol{x_0})^\mathsf{T}\vec{\boldsymbol{n}}}{\|\mathbf{D\Phi}(\boldsymbol{x_0})^\mathsf{T}\vec{\boldsymbol{n}}\|} \,.$$

COROLLARY 5.4. *Let $Z_{\mathbf{\Phi},X}$ be a WAFBF formed by a standard elementary field X with anisotropy function (5.2) and the deformation function (5.3) satisfying (5.4), we have that at each point $\boldsymbol{x_0}$, $Z_{\mathbf{\Phi},X}$ admits as local orientation $\vec{\boldsymbol{n}}(\boldsymbol{x_0}) = \mathbf{D\Phi}(\boldsymbol{x_0})^\mathsf{T}(1,0)^\mathsf{T}$, that is*

$$\vec{\boldsymbol{n}}(\boldsymbol{x_0}) = \boldsymbol{u}(\alpha(\boldsymbol{x_0})) + \langle \boldsymbol{u}(\alpha(\boldsymbol{x_0}))^\perp, \boldsymbol{x_0} \rangle \nabla\alpha(\boldsymbol{x_0}) \,.$$

with $\boldsymbol{u}(\alpha(\boldsymbol{x_0})) = (\cos(\alpha_0(\boldsymbol{x_0})), \sin(\alpha_0(\boldsymbol{x_0}))$.

Notice that this random field has local orientations which are not $\boldsymbol{u}(\alpha(\boldsymbol{x_0}))$, it depends on the gradient $\nabla\alpha$, so this is not a practical way to control the prescribed orientation. However, another way to construct a deformation field which leads to the proper orientation $\boldsymbol{u}(\alpha(\boldsymbol{x_0}))$, is based on conformal mapping. More precisely, we proved in [39] the following result:

COROLLARY 5.5. *Let α be an harmonic function defined on $\mathbb{R}^2$. Then there exists some λ such that $\mathbf{\Psi} = \begin{pmatrix} \lambda \\ -\alpha \end{pmatrix}$ is continuously differentiable and satisfied the Cauchy–Riemann equation. Let $\mathbf{\Phi}$ be any primitive of $\exp(\mathbf{\Psi})$ as an holomorphic function on $\mathbb{C}$. At any point $\boldsymbol{x_0}$, the local orientation of $Z_{\mathbf{\Phi},X}$ is*

$$\vec{\boldsymbol{n}}_Z(\boldsymbol{x_0}) = \begin{pmatrix} \cos\alpha(\boldsymbol{x}) \\ \sin\alpha(\boldsymbol{x}) \end{pmatrix} \,.$$

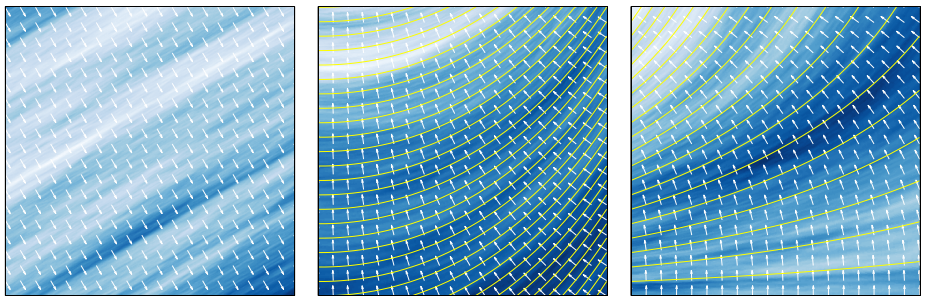

(a) $(a, b, c) = (2, -1, 0)$ (b) $(a, b, c) = (1, 0, \pi/2)$ (c) $(a, b, c) = (0, 1, \pi/2)$

Fig. 14: Simulation of the field $Z(\boldsymbol{x}) = X(\boldsymbol{\Phi}(\boldsymbol{x}))$, where X is the standart elementary field and the harmonic function $\alpha(x_1, x_2) = ax_1 + bx_2 + c$, with their level lines.

Let us now characterize the level lines corresponding to the vector field $\vec{\boldsymbol{n}}_Z(\boldsymbol{x_0})$, which also corresponds to the integral curve of the vector field V defined by

$$\boldsymbol{V} : (x, y) \mapsto (-\sin\alpha(x, y), \cos\alpha(x, y)) \ .$$

Let $\gamma : t \in \mathbb{R} \mapsto (\gamma_1(t), \gamma_2(t))$ be a parametrized curve on $\mathbb{R}^2$, then integral curve passing through the point (x_0, y_0) is given by

$$\begin{cases} \frac{\mathrm{d}\gamma}{\mathrm{d}t} = \boldsymbol{V}(\gamma(t)) \\ \gamma(0) = (x_0, y_0) \end{cases} \iff \begin{cases} \frac{\mathrm{d}\gamma_1}{\mathrm{d}t} = -\sin\alpha(\gamma_1(t), \gamma_2(t)) \\ \gamma_1(0) = x_0 \\ \frac{\mathrm{d}\gamma_2}{\mathrm{d}t} = \cos\alpha(\gamma_1(t), \gamma_2(t)) \\ \gamma_2(0) = y_0 \end{cases} .$$

Reformulated with a one dimensional function, we are looking for f such that $\gamma(t) = (t, f(t))$ and

$$\begin{cases} f'(t) = -\mathrm{cotan}\,\alpha(t, f(t)) \\ f(0) = y_0 \end{cases} .$$

In the particular of harmonic functions $\alpha_1(x, y) = x - \frac{\pi}{2}$ and $\alpha_2(x, y) = y - \frac{\pi}{2}$, one can easily show that the parametric function searched is respectively

$$\begin{cases} f_1(x) = \ln\left|\dfrac{1}{\cos x}\right| + y_0 \\ f_2(x) = \arcsin(\sin(y_0)\mathrm{e}^x) \end{cases} .$$

We superposed in Figure 14 these curves with corresponding textures simulating the associated WAFBF.

6. Estimation of the elementary field anisotropy. In this section, we propose a method to estimate the vector orientation $\vec{\boldsymbol{n}}_X$ of an elementary field $X = Y_{H,\alpha_0-\delta,\alpha_0+\delta}$ and to characterize its statistic distribution. More precisely, from the Riesz wavelet coefficients $c^{(\ell)}_{i,\boldsymbol{k}}(X) = \langle X, \mathcal{R}_\ell\psi_{i,\boldsymbol{k}}\rangle$, we have determined in Theorem 3.3 the covariance of the Riesz wavelet vector $c^{(\mathcal{R})}_{i,\boldsymbol{k}}(X) = (c^{(1)}_{i,\boldsymbol{k}}(X), c^{(2)}_{i,\boldsymbol{k}}(X))^\mathsf{T}$. The vector orientation can be estimated using this correlation between the components of wavelet coefficients, performing a linear regression along scales i, in order to evaluate H and

the tensor structure $\mathbf{J}(X)$. Then, the unit eigenvector corresponding to the largest eigenvalue provides an estimation of the vector orientation $\vec{\boldsymbol{n}}_X = (\cos\alpha_0, \sin\alpha_0)^\mathsf{T}$.

Alternatively, one can define an unit orientation vector in the pixel $\boldsymbol{k} = (k_1, k_2)$ at scale i as

$$\vec{\boldsymbol{n}}_{i,\boldsymbol{k}} = \frac{c^{(\mathcal{R})}_{i,\boldsymbol{k}}(X)}{\left|c^{(\mathcal{R})}_{i,\boldsymbol{k}}(X)\right|} = \frac{1}{\sqrt{c^{(1)}_{i,\boldsymbol{k}}(X)^2 + c^{(2)}_{i,\boldsymbol{k}}(X)^2}} \begin{pmatrix} c^{(1)}_{i,\boldsymbol{k}}(X) \\ c^{(2)}_{i,\boldsymbol{k}}(X) \end{pmatrix} = \begin{pmatrix} \cos\alpha_{i,\boldsymbol{k}}(X) \\ \sin\alpha_{i,\boldsymbol{k}}(X) \end{pmatrix} ,$$

with

$$\alpha_{i,\boldsymbol{k}}(X) = \operatorname{atan}\left(\frac{c^{(2)}_{i,\boldsymbol{k}}(X)}{c^{(1)}_{i,\boldsymbol{k}}(X)}\right) ,$$

which give a *local* estimation of the orientation at this position and scale. So now, one can look for the angle distribution of the random variable $\alpha_{i,\boldsymbol{k}}$ in order to estimate the orientation of the elementary field X. Proposition 6.2 shows that the density function of $\alpha_{i,\boldsymbol{k}}$ does not depends on the scale i, the position $\boldsymbol{k}$, the wavelet ψ, nor the Hurst index H. It only depends on the constant parameters α_0 and δ of the anisotropy function $c_{\alpha_0,\delta}$. Then, we show that the peaks density is centered on the searched orientation α_0 and the maximum likelihood provides an estimator of this orientation.

LEMMA 6.1. *Let be a Gaussian vector $\boldsymbol{X} = (X_1, X_2)$ characterized by the covariance matrix $\boldsymbol{\Sigma}$, which can be factorized as $\boldsymbol{\Sigma} = \mathbf{M}\mathbf{M}^\mathsf{T}$ with*

$$\mathbf{M} = \begin{pmatrix} a & b \\ c & d \end{pmatrix}, \quad \det\mathbf{M} > 0 .$$

Then, the random variable X_1/X_2 follows a Cauchy distribution C_z of complex parameter $z = (a\mathrm{j} + b)/(c\mathrm{j} + d)$.

Proof. The variance-covariance matrix $\boldsymbol{\Sigma}$, which is definite positive, can always be factorized such a way, for example by the Cholesky decomposition. From this decomposition, given a vector $\boldsymbol{Z} = (Z_1, Z_2)$ with Z_1, Z_2 two i.i.d $\mathcal{N}(0,1)$, we have $\boldsymbol{X} \sim \mathbf{M}\boldsymbol{Z}$. Besides, the variable $Q = Z_1/Z_2$ follows a standard Cauchy distribution C_j. Recall that a Cauchy distribution C_z of complex parameter $z = p + \mathrm{j}q$ with $q > 0$, has the probability density function $x \mapsto q/\pi((x-p)^2 + q^2)$. So, from $\boldsymbol{X} \sim \mathbf{M}\boldsymbol{Z}$, we obtain

$$\frac{X_1}{X_2} \sim \frac{aQ + b}{cQ + d} = r(Q) .$$

From a theorem of [26] and reference therein, if $Q \sim C_z$ then $r(Q) \sim C_{r(z)}$. Applied for $z = \mathrm{j}$ and we get that X_1/X_2 follows a Cauchy distribution of parameter $r(\mathrm{j})$, that is the sought after result. ∎

PROPOSITION 6.2. *Let X be an elementary field with anisotropy function*

$$C_X(\boldsymbol{\Theta}) = \frac{1}{4\delta}\left(\mathbb{1}_{[-\delta,\delta]}(\arg\boldsymbol{\Theta}) + \mathbb{1}_{[\pi-\delta,\pi+\delta]}(\arg\boldsymbol{\Theta})\right) ,$$

and $c^{(\mathcal{R})}_{i,\boldsymbol{k}}(X) = \left(c^{(1)}_{i,\boldsymbol{k}}(X), c^{(2)}_{i,\boldsymbol{k}}(X)\right)^\mathsf{T}$ in the vector wavelet tight frame $\{\mathcal{R}\psi_{i,\boldsymbol{k}}\}$, defined in (3.2) from an isotropic wavelet $\widehat{\psi}(\boldsymbol{\xi}) = \varphi(\|\boldsymbol{\xi}\|)$.
The covariance matrix of the $c^{(\mathcal{R})}_{i,\boldsymbol{k}}(X)$ is known by Theorem 3.3

$$\boldsymbol{\Sigma}\left(c^{(\mathcal{R})}_{i,\boldsymbol{k}}(X)\right) = 2^{-2i(H+1)} c_\psi \mathbf{J}(X) , \quad \textit{with} \quad c_\varphi = \left[\int_0^{+\infty} \frac{|\varphi(r)|^2}{r^{2H+1}}\,\mathrm{d}r\right] ,$$

and with the tensor structure $\mathbf{J}(X)$ *whose expression is given in* (3.5) *by*

$$\mathbf{J}(X) = \mathbf{R}_{\alpha_0} \mathrm{diag}\left(\frac{1}{2} + \frac{1}{2}\frac{\sin(2\delta)}{2\delta}, \frac{1}{2} - \frac{1}{2}\frac{\sin(2\delta)}{2\delta}\right) \mathbf{R}_{\alpha_0}^{\mathsf{T}} .$$

Let us define the random variable

$$\Omega_{i,\boldsymbol{k}}(X) = \frac{c_{i,\boldsymbol{k}}^{(1)}(X)}{c_{i,\boldsymbol{k}}^{(2)}(X)} .$$

1. *The probability density function of* $\Omega_{i,\boldsymbol{k}}$ *is*

$$f_\Omega(x;\alpha_0,\delta) = \frac{q(\alpha_0,\delta)}{\pi\left[(x-p(\alpha_0,\delta))^2 + q(\alpha_0,\delta)^2\right]} , \tag{6.1}$$

with

$$p(\alpha_0,\delta) = \frac{\mathrm{sinc}(2\delta)\sin(2\alpha_0)}{1-\mathrm{sinc}(2\delta)\cos(2\alpha_0)}, \quad q(\alpha_0,\delta) = \frac{\sqrt{1-\mathrm{sinc}^2(2\delta)}}{1-\mathrm{sinc}(2\delta)\cos(2\alpha_0)} .$$

which does not depends on the scale i*, the wavelet* ψ*, nor the Hurst index* H*.*

2. *The probability density function of* $\alpha_{i,\boldsymbol{k}} = \arctan\left(\frac{1}{\Omega_{i,\boldsymbol{k}}}\right)$ *is*

$$\begin{aligned} f_\alpha(x;\alpha_0,\delta) &= (1+\mathrm{cotan}^2 x) f_\Omega(\mathrm{cotan}\, x;\alpha_0,\delta) , \\ &= \frac{q(\alpha_0,\delta)(1+\mathrm{cotan}^2 x)}{\pi[(\mathrm{cotan}\, x - p(\alpha_0,\delta))^2 + q(\alpha_0,\delta)^2]} . \end{aligned} \tag{6.2}$$

Proof. We apply Lemma 6.1 to the Gaussian vector $c_{i,\boldsymbol{k}}^{(\mathcal{R})}(X)$ and the variance-covariance matrix $\mathbf{\Sigma}_i = 2^{-2i(H+1)} c_\psi \mathbf{J}(X)$ that we can factorize as $\mathbf{\Sigma}_i = \mathbf{M}\mathbf{M}^{\mathsf{T}}$ with

$$\mathbf{M} = 2^{-i(H+1)} c_\psi^{1/2} \mathbf{R}_{\alpha_0} \mathrm{diag}\left(\sqrt{\frac{1}{2} + \frac{1}{2}\mathrm{sinc}(2\delta)}, \sqrt{\frac{1}{2} - \frac{1}{2}\mathrm{sinc}(2\delta)}\right) ,$$

that is

$$\mathbf{M} = 2^{-i(H+1)} c_\psi^{1/2} \begin{pmatrix} \cos\alpha_0 \sqrt{\frac{1}{2} + \frac{1}{2}\mathrm{sinc}(2\delta)} & -\sin\alpha_0 \sqrt{\frac{1}{2} - \frac{1}{2}\mathrm{sinc}(2\delta)} \\ \sin\alpha_0 \sqrt{\frac{1}{2} + \frac{1}{2}\mathrm{sinc}(2\delta)} & \cos\alpha_0 \sqrt{\frac{1}{2} - \frac{1}{2}\mathrm{sinc}(2\delta)} \end{pmatrix} ,$$

and

$$\det \mathbf{M} = 2^{-2i(H+1)} \frac{c_\psi}{2} \sqrt{1-\mathrm{sinc}^2(2\delta)} > 0, \quad \text{for } \delta > 0 .$$

Consequently, we have that $\Omega_{i,\boldsymbol{k}} \sim C_{z(\alpha,\delta)}$ with the complex parameter

$$z(\alpha_0,\delta) = \frac{\cos\alpha_0 \sqrt{\frac{1}{2} + \frac{1}{2}\mathrm{sinc}(2\delta)}\mathrm{j} - \sin\alpha_0 \sqrt{\frac{1}{2} - \frac{1}{2}\mathrm{sinc}(2\delta)}}{\sin\alpha_0 \sqrt{\frac{1}{2} + \frac{1}{2}\mathrm{sinc}(2\delta)}\mathrm{j} + \cos\alpha_0 \sqrt{\frac{1}{2} - \frac{1}{2}\mathrm{sinc}(2\delta)}} = p(\alpha_0,\delta) + \mathrm{j}q(\alpha_0,\delta) ,$$

with

$$p(\alpha_0,\delta)=\frac{\operatorname{sinc}(2\delta)\sin(2\alpha_0)}{1-\operatorname{sinc}(2\delta)\cos(2\alpha_0)},\quad q(\alpha_0,\delta)=\frac{\sqrt{1-\operatorname{sinc}^2(2\delta)}}{1-\operatorname{sinc}(2\delta)\cos(2\alpha_0)}\,.$$

Therefore, we deduce (6.1). To prove (6.2), we now characterize the cumulative distribution of $\alpha_{i,\boldsymbol{k}}$, since $\arctan(x)+\arctan\left(\frac{1}{x}\right)=\operatorname{sgn}(x)\frac{\pi}{2}$ we have

$$\begin{aligned}F_\alpha(x)&=\mathbb{P}(\alpha_{i,\boldsymbol{k}}\leqslant x)\,,\\&=\mathbb{P}(\arctan\left(1/\Omega_{i,\boldsymbol{k}}\right)\leqslant x)\,,\\&=1-\mathbb{P}(\Omega_{i,\boldsymbol{k}}\leqslant\operatorname{cotan}x)\,,\\&=1-F_\Omega(\operatorname{cotan}x)\,.\end{aligned}$$

By differentiating we obtain (6.2) the probability density function of $\alpha_{i,\boldsymbol{k}}$, for all $-\frac{\pi}{2}\leqslant x\leqslant\frac{\pi}{2}$. ∎

Remark 6.3. One can verify, by computing $f'_\alpha(x;\alpha_0,\delta)=0$ (which comes down to a quadratic equation), that the maximal value of f_α is achieved for $x=\alpha_0$.

Appendix A. Cholesky method. Hereafter we recall a classic way to simulate a Gaussian vector $\boldsymbol{X}=(X_1,\dots,X_N)$ of size N such that $\mathbb{E}[X_i]=0$ for all i, is completely determined by its covariance $\mathbf{R}$ of size $N\times N$ whose coefficients are $\mathbf{R}_{ij}=\operatorname{Cov}(X_i,X_j)$. To this end, we use the Cholesky decomposition of $\mathbf{R}$ i.e. $\mathbf{R}=\mathbf{L}\mathbf{L}^\mathsf{T}$. Note that it is possible to obtain a Cholesky decomposition of $\mathbf{R}$ since by definition the covariance matrix $\mathbf{R}$ is symmetric and positive definite. Now take a random vector, $\boldsymbol{Z}\sim\mathcal{N}(\mathbf{0},\mathbf{I})$, consisting of uncorrelated random variables with each random variable, Z_i, having zero mean and unit variance 1. Since Z_i's are uncorrelated random variables with zero mean and unit variance, we have $\mathbb{E}\left[Z_iZ_j\right]=\delta_{ij}$. Hence,

$$\mathbb{E}\left[\boldsymbol{Z}\boldsymbol{Z}^\mathsf{T}\right]=\mathbf{I}\,.$$

Set now $\boldsymbol{X}=\mathbf{L}\boldsymbol{Z}$. Taking into account the fact that this vector is centered, we can now explicit its covariance matrix

$$\mathbb{E}\left[\boldsymbol{X}\boldsymbol{X}^\mathsf{T}\right]=\mathbb{E}\left[(\mathbf{L}\boldsymbol{Z})(\mathbf{L}\boldsymbol{Z})^\mathsf{T}\right]=\underbrace{\mathbb{E}\left[\mathbf{L}\boldsymbol{Z}\boldsymbol{Z}^\mathsf{T}\mathbf{L}^\mathsf{T}\right]=\mathbf{L}\mathbb{E}\left[\boldsymbol{Z}\boldsymbol{Z}^\mathsf{T}\right]\mathbf{L}^\mathsf{T}}_{\text{Since expectation is a linear operator}}=\mathbf{L}\mathbf{I}\mathbf{L}^\mathsf{T}=\mathbf{L}\mathbf{L}^\mathsf{T}=\mathbf{R}$$

Hence, the random vector $\boldsymbol{X}$ has the desired covariance matrix, $\mathbf{R}$.

Appendix B. Proof of Proposition 4.5. The predicted error has the following variance:

$$\begin{aligned}\operatorname{Var}\left[\widehat{Z}(\boldsymbol{s_0})-Z(\boldsymbol{s_0})\right]&=\operatorname{Var}\left[\boldsymbol{\lambda}^\mathsf{T}\mathbf{Z}-Z(s_0)\right]\,,\\&=\operatorname{Var}\left[\boldsymbol{\lambda}^\mathsf{T}\mathbf{Z}\right]+\operatorname{Var}\left[Z(\boldsymbol{s_0})\right]-2\operatorname{Cov}\left[\boldsymbol{\lambda}^\mathsf{T}\mathbf{Z},Z(\boldsymbol{s_0})\right]\,,\\&=\boldsymbol{\lambda}^\mathsf{T}\operatorname{Var}\left[\mathbf{Z}\right]\boldsymbol{\lambda}+\operatorname{Var}\left[Z(\boldsymbol{s_0})\right]-2\boldsymbol{\lambda}^\mathsf{T}\operatorname{Cov}\left[\mathbf{Z},Z(\boldsymbol{s_0})\right]\,,\\&=\boldsymbol{\lambda}^\mathsf{T}\boldsymbol{\Sigma}\boldsymbol{\lambda}+\sigma^2-2\boldsymbol{\lambda}^\mathsf{T}\boldsymbol{c_0}\,,\\&=J(\boldsymbol{\lambda})\end{aligned}$$

where $\sigma^2=\operatorname{Var}[Z(\boldsymbol{s_0})]$ and $\boldsymbol{c_0}=\operatorname{Cov}[\mathbf{Z},Z(\boldsymbol{s_0})]$, vector of size $1\times n_0$.

To minimize the function $J(\boldsymbol{\lambda})$ we compute its gradient:

$$\nabla J(\boldsymbol{\lambda}) = 2\boldsymbol{\Sigma}\boldsymbol{\lambda} - 2\boldsymbol{c_0} \ ,$$

which is a null vector for

$$\widehat{\boldsymbol{\lambda}} = \boldsymbol{\Sigma}^{-1}\boldsymbol{c_0} \ .$$

Moreover the Hessian matrix is $2\boldsymbol{\Sigma}$ which is semi-definite positive (since it is a variance-covariance matrix), hence $J(\boldsymbol{\lambda})$ is a convex function and the critical point $\widehat{\boldsymbol{\lambda}} = \boldsymbol{\Sigma}^{-1}\boldsymbol{c_0}$ is a global minimum.

Thus, the prediction $\widehat{Z}(\boldsymbol{s_0})$ of $Z(\boldsymbol{s_0})$ is given by:

$$\widehat{Z}(\boldsymbol{s_0}) = \boldsymbol{c_0}^{\mathsf{T}}\boldsymbol{\Sigma}^{-1}\mathbf{Z} \ .$$

REFERENCES

[1] A. Ayache, *The generalized multifractional field: a nice tool for the study of the generalized multifractional Brownian motion*, Journal of Fourier Analysis and Applications, 8 (2002), pp. 581–602.

[2] A. Ayache and J. Hamonier, *Linear multifractional stable motion: fine path properties*, Revista Matematica Iberoamericana, (2014).

[3] A. Ayache and J. Lévy Véhel, *The generalized multifractional Brownian motion.*, Statistical Inference for Stochastic Processes, 3 (2000), pp. 7–18.

[4] A. Benassi, S. Jaffard, and D. Roux, *Elliptic Gaussian random processes*, Revista Matemática Iberoamericana, 13 (1997), pp. 19–90.

[5] A. Benassi, S. Jaffard, and D. Roux, *Elliptic Gaussian random processes*, Revista Matematica Iberoamericana, 13 (1997), pp. 19–90.

[6] D. Benson, M. Meerschaert, B. Baumer, and H. Scheffler, *Aquifer operator-scaling and the effect on solute mixing and dispersion*, Water Resour.Res., W01415 (2006), pp. 1–18.

[7] H. Biermé, L. Moisan, and F. Richard, *A turning-band method for the simulation of anisotropic fractional brownian fields*, Journal of Computational and Graphical Statistics, 24 (2015), pp. 885–904.

[8] P. Billingsley, *Convergence of probability measure*, John Wiley and Sons, (1968).

[9] A. Bonami and A. Estrade, *Anisotropic analysis of some Gaussian models*, Journal of Fourier analysis and applications, 9 (2003), pp. 215–236.

[10] A. Brouste, J. Istas, and S. Lambert-Lacroix, *On fractional Gaussian random fields simulations*, Journal of Statistical Software, 23 (2007), pp. 1–23.

[11] G. Chan and A. T. Wood, *Simulation of multifractional Brownian motion*, in COMPSTAT, Springer, 1998, pp. 233–238.

[12] R. Chellappa, R. Kashyap, and B. Manjunath, *Model-based texture segmentation and classification*, in Handbook of pattern recognition & computer vision, World Scientific Publishing Co., Inc., 1993, pp. 277–310.

[13] R. B. Davies and D. Harte, *Tests for Hurst effect*, Biometrika, 74 (1987), pp. 95–101.

[14] S. Davies and P. Hall, *Fractal analysis of surface roughness by using spatial data (with discussion)*, J. Roy. Statist. Soc. Ser., B 61 (1999), pp. 3–37.

[15] C. Dietrich and G. N. Newsam, *Fast and exact simulation of stationary Gaussian processes through circulant embedding of the covariance matrix*, SIAM Journal on Scientific Computing, 18 (1997), pp. 1088–1107.

[16] K. Falconer, *Tangent Fields and the local structure of random fields*, J.Theo.Prob., 15 (2002), pp. 731–750.

[17] K. Falconer, *The local structure of random processes*, J.London Math. Soc., 67 (2003), pp. 657–672.

[18] R. Haralick, *Statistical and structural approaches to texture*, Proceedings of the IEEE, 67 (1979), pp. 786–804.

[19] S. Held, M. Storah, P. Massopust, and B. Forster, *Steerable wavelet frames based on the Riesz transform*, IEEE Trans. Image Process., 19 (2010), pp. 653–667.

[20] E. Herbin, *From N–parameter fractional Brownian motions to N–parameter multifractional Brownian motions*, Rocky Mountain J. of Math., 36 (2006), pp. 1249–1284.

[21] W. Hudson and J. Mason, Trans. Am. Math. Soc., 273 (1982), pp. 281–297.
[22] B. Julesz, *Visual pattern discrimination*, IEEE Trans. Information Theory, 8 (1962), pp. 84–92.
[23] B. Julesz, E. Gilbert, L. Shepp, and H. Frisch, *Inability of humans to discriminate between visual textures that agree in second-order statistics revisited*, Perception, 2 (1973), pp. 391–405.
[24] A. Kamont, *On the fractional anisotropic wiener field*, Probability and Mathematical Statistics-PWN, 16 (1995), pp. 85–98.
[25] D. Kbiob, *A statistical approach to some basic mine valuation problems on the witwatersrand*, Journal of Chemical, Metallurgical, and Mining Society of South Africa, (1951).
[26] G. Letac, *Which functions preserve cauchy laws?*, Proceedings of the American Mathematical Society, 67 (1977), pp. 277–286.
[27] J. Lévy-Vehel and R. Peltier, *Multifractional Brownian Motion : definition and preliminary results*, Research Report RR-2645, INRIA, 1995.
[28] B. Mandelbrot and J. Van Ness, *Fractional Brownian motions, fractional noises and applications*, SIAM review, 10 (1968), pp. 422–437.
[29] G. Matheron, *Traité de géostatistique appliquée*, vol. 1, Editions Technip, 1962.
[30] G. Matheron, *Principles of geostatistics*, Economic geology, 58 (1963), pp. 1246–1266.
[31] G. Matheron, *Traité de géostatistique appliquée, le krigeage. mémoires du bureau de recherches géologiques et minières*, 1963.
[32] P. Maurel, J. Aujol, and G. Peyré, *Locally parallel texture modeling*, SIAM Journal on Imaging Sciences, 4 (2011), pp. 413–447.
[33] P. O. and S. R., *Reducing non-stationary random fields to stationarity and isotropy using a space deformation*, Statistics and Probability Letters, 48 (2000), pp. 23–32.
[34] M. Papadakis, G. Gogoshin, I. Kakadiaris, D. Kouri, and D. Hoffman, *Nonseparable radial frame multiresolution analysis in multidimensions*, Numer. Funct. Anal. Optim., 24 (2003), pp. 907–928.
[35] R. Peltier, J. Véhel, et al., *Multifractional Brownian motion: definition and preliminary results*, (1995).
[36] E. Perrin, R. Harba, R. Jennane, and I. Iribarren, *Fast and exact synthesis for 1-D fractional Brownian motion and fractional Gaussian noises*, IEEE Signal Processing Letters, 9 (2002), pp. 382–384.
[37] K. Polisano, M. Clausel, V. Perrier, and L. Condat, *Texture Modeling by Gaussian fields with prescribed local orientation*, IEEE International Conference on Image Processing (ICIP), Paris, 27-30 Oct., (2014), pp. 6091–6095.
[38] K. Polisano, M. Clausel, V. Perrier, and L. Condat, *Modélisation de texture par champ gaussien à orientation locale prescrite*, in XXVème colloque GRETSI sur le Traitement du Signal et des Images, Lyon, 2015.
[39] K. Polisano, M. Clausel, V. Perrier, and L. Condat, *Wavelet-based orientation of localisable Gaussian fields*, Technical report, hal-01570978, (2017).
[40] J. Portilla and E. Simoncelli, *A parametric texture model based on joint statistics of complex wavelet coefficients*, Int. J. Comput. Vis., 40 (2000), pp. 49–70.
[41] T. Reed and J. H. Dubuf, *A review of recent texture segmentation and feature extraction techniques*, CVGIP: Image understanding, 57 (1993), pp. 359–372.
[42] F. J. Richard, *Tests of isotropy for rough textures of trended images*, Statistica Sinica, (2016), pp. 1279–1304.
[43] J. Romero, S. Alexander, S. Baid, S. Jain, and M. Papadakis, *The geometry and the analytic properties of isotropic multiresolution analysis*, Adv. Comput. Math., 31 (2009), pp. 283–328.
[44] S. Roux, M. Clausel, B. Vedel, and P. Jaffard, S. Abry, *The hyperbolic wavelet transform for self–similar anisotropic texture analysis*, IEEE Trans. Imag. Proc., 22 (2013), pp. 4353–4363.
[45] R. Shapiro, H. L.G., and R. Haralick, *Computer and robot vision*, Reading: Addison-Wesley, (1992).
[46] M. L. Stein, *Fast and exact simulation of fractional Brownian surfaces*, Journal of Computational and Graphical Statistics, 11 (2002), pp. 587–599.
[47] M. Tuceryan and A. Jain, *Texture analysis, handbook of pattern recognition and computer vision*, (1993), pp. 235–276.
[48] M. Unser and N. Chenouard, *A Unifying Parametric Framework for 2D Steerable Wavelet Transforms*, SIAM Journal on Imaging Sciences, 6 (2013), pp. 102–135.
[49] M. Unser, N. Chenouard, and D. Van De Ville, *Steerable Pyramids and Tight Wavelet Frames in $L^2(\mathbb{R}^d)$*, IEEE Trans. Image Process., 20 (2011), pp. 2705–2721.

[50] D. Van De Ville, T. Blu, and M. Unser, *Isotropic polyharmonic B–splines: Scaling functions and wavelets*, IEEE Trans. Image Process., 14 (2005), pp. 1798–1813.
[51] L. Van Gool, P. Dewaele, and A. Oosterlinck, *Texture analysis anno 1983*, Computer vision, graphics, and image processing, 29 (1985), pp. 336–357.
[52] A. T. Wood and G. Chan, *Simulation of stationary Gaussian processes in [0, 1]*, Journal of computational and graphical statistics, 3 (1994), pp. 409–432.